AIMS Mathematics, 11(2): 5029–5061.
DOI: 10.3934/math.2026206
Received: 01 October 2025
Revised: 23 January 2026
Accepted: 26 January 2026
Published: 27 February 2026

https://www.aimspress.com/journal/Math

Research article

A hybrid approach to diabetes modeling: Fractional derivatives and stochastic analysis

Sayed Saber[1,2,*], **Emad Solouma**[3], **A. F. Aljohani**[4] **and Faisal Muteb K. Almalki**[1]

[1] Department of Mathematics, Faculty of Science, Al-Baha University, Alaqiq, 65779–7738, Saudi Arabia

[2] Department of Mathematics and Computer Science, Faculty of Science, Beni-Suef University, Egypt

[3] Department of Mathematics and Statistics, College of Science, Imam Mohammad Ibn Saud Islamic University (IMSIU), Saudi Arabia

[4] Department of Mathematics, Faculty of Science, University of Tabuk, Tabuk, Saudi Arabia

* **Correspondence:** Email: Sayed011258@science.bsu.edu.eg.

Abstract: In this study, the Michaelis-Menten function was incorporated into a fractional stochastic model of glucose-insulin degradation to describe insulin degradation. The existence, uniqueness, boundedness, and nonnegativity properties of the model were derived through rigorous mathematical analysis. This paper presented an analysis of stability, including asymptotic and Hyers-Ulam stability. By integrating stochastic perturbations into fractional differential equations with Caputo derivatives, we enhanced the realism of diabetes modeling. A stochastic Runge-Kutta method of type 4 was employed to solve the system, ensuring improved accuracy and stability in simulating glucose-insulin dynamics under random fluctuations. Through sensitivity analysis, four optimized control strategies, including insulin injection regimens and pharmaceutical interventions, were identified. An analysis of the dynamic behavior of the system under various physiological conditions was carried out using fractional Predictor-Evaluator-Corrector-Evaluator (PECE) methods of Adams-Bashford-Moulton type and Runge-Kutta type 4. Based on the results, it appeared that fractional stochastic modeling could capture long-term memory effects and inherent randomness in glucose metabolism, thereby providing a more comprehensive framework for diabetes management and prediction.

Keywords: fractional calculus; glucose-insulin model; stochastic differential equations; Michaelis-Menten kinetics; Hyers-Ulam stability; Predictor-corrector method; Runge-Kutta method; sensitivity analysis; diabetes management
Mathematics Subject Classification: 26A33, 34A08, 34F05, 65L05, 92C45, 93C95

1. Introduction

Understanding the interplay between glucose and insulin necessitates advanced mathematical models for better disease management. Carbohydrates derived from sources such as grains, meat, and dairy are essential for cellular energy. Certain tissues, including the brain, require insulin for glucose uptake, whereas others, like muscle tissue, can absorb glucose independently. The pancreas, through its beta cells, is responsible for insulin production. This hormone facilitates glucose metabolism, ensuring efficient energy utilization.

The plasma glucose concentration at time t, denoted by $\mathtt{X}(t)$, is measured in milligrams per deciliter (mg/dL). Parameters $\mathtt{X}_{in}$ and $\mathtt{Y}_{in}$ govern plasma insulin concentration by specifying glucose intake and external insulin infusion rates. These constants play a critical role in maintaining metabolic equilibrium. The function of $\mathtt{X}(t)$ is crucial as it ensures a stable energy supply for cells, while $\mathtt{Y}(t)$, representing insulin levels, regulates glucose absorption and prevents extreme blood sugar fluctuations. Together, these variables maintain metabolic homeostasis and ensure physiological stability.

Several glucose-insulin models postulate that insulin clearance follows a proportional relationship with its concentration [1–4]. However, overly simplistic assumptions may compromise diagnostic accuracy and treatment efficacy. As noted in [4], an abundance of resources does not indefinitely accelerate metabolic rates. To account for this, their model incorporated the Michaelis-Menten function $\frac{d\mathtt{Y}}{e+\mathtt{Y}}$ to describe insulin degradation. Here, d represents the maximum insulin clearance rate, while e denotes the half-saturation constant. This formulation, which deviates from traditional linear models, offers a more realistic representation of physiological processes.

Building upon the work in [4, 5], this study introduces a refined glucose-insulin model that integrates a nonlinear insulin degradation rate based on the Michaelis-Menten function. Unlike previous models that assume a linear clearance rate, this approach more accurately reflects physiological behavior. Traditional models may oversimplify the dynamics, leading to less precise predictions. By incorporating nonlinear degradation, our framework enhances the understanding of glucose-insulin interactions, offering potential improvements in treatment strategies for metabolic disorders.

$$\begin{aligned} \frac{\mathrm{d}\mathtt{X}}{\mathrm{d}t} &= \mathtt{X}_{in} - a\mathtt{X} - b\mathtt{X}\mathtt{Y}, \quad \mathtt{X}(0) > 0, \\ \frac{\mathrm{d}\mathtt{Y}}{\mathrm{d}t} &= \mathtt{Y}_{in} + c\mathtt{X} - \frac{d\,\mathtt{Y}}{e+\mathtt{Y}}, \quad \mathtt{Y}(0) > 0. \end{aligned} \tag{1.1}$$

Table 1 summarizes the biological significance of the parameters in the stochastic fractional glucose-insulin model. The interpretations are as follows: $\mathtt{X}_{in}$ represents the glucose intake rate, describing the entry of glucose into the bloodstream from dietary consumption. $\mathtt{Y}_{in}$ signifies the rate of externally administered insulin. The parameter a quantifies glucose consumption by insulin-independent tissues such as the brain, while b accounts for insulin-dependent tissue uptake, including muscle cells. The rate of insulin secretion in response to glucose is denoted by c, while d and e correspond to the maximum insulin clearance rate and half-saturation level, respectively.

Table 1. Model parameters and their values [4, 5].

Parameter	Definition	Units	Assigned Values
G_{in}	Glucose ingestion rate	mg/dl/min	4.5
I_{in}	Rate of external insulin administration	μU/ml/min	[0, 3, 6, 10]
a	Basal glucose consumption rate	min^{-1}	0.0002
b	Glucose utilization due to insulin	ml/μU/min	7.5919e-4
c	Insulin production coefficient	μU/ml/min/(mg/dl)	0.2298
d	Peak insulin elimination rate	μU/ml/min	1500
e	Half-max saturation constant	-	2300

Recent research efforts have focused on developing mathematical models based on intravenous glucose tolerance tests (IVGTT) to analyze glucose-insulin interactions [6–12]. The role of epidemiological modeling extends beyond medicine, contributing significantly to various fields such as engineering, physics, economics, and chemistry [13–36].

Fractional calculus has proven to be a valuable tool for capturing complex biological dynamics, particularly in systems that exhibit memory and hereditary properties. This study employs fractional calculus to construct an advanced glucose-insulin model, incorporating the Michaelis-Menten framework for insulin degradation. The fractional approach provides a more nuanced representation of diabetes pathology, offering insights into long-term glucose and insulin fluctuations. Moreover, fractional differential equations have found applications in modeling intricate physiological systems. For instance, the cardiovascular system has been analyzed using fractional models to describe anomalous blood flow diffusion and the viscoelastic behavior of arterial walls. Such methodologies enable more accurate predictions and simulations of heart-related disorders. Despite these advantages, applying the Caputo fractional derivative to real-world medical challenges remains a nontrivial task.

The primary objective of this study is to analyze the fractional-order mathematical framework and dynamics of a glucose-insulin system (1.1) utilizing the Caputo fractional derivative approach.

$$\begin{aligned} \mathscr{D}_t^{\nu}\mathtt{X}(t) &= \mathtt{X}_{in} - a\mathtt{X} - b\mathtt{X}\mathtt{Y}, \qquad \mathtt{X}(0) = \mathtt{X}_0, \\ \mathscr{D}_t^{\nu}\mathtt{Y}(t) &= \mathtt{Y}_{in} + c\mathtt{X} - \frac{d\,\mathtt{Y}}{e+\mathtt{Y}}, \qquad \mathtt{Y}(0) = \mathtt{Y}_0. \end{aligned} \tag{1.2}$$

The properties of uniqueness, nonnegativity, and boundedness of the solutions are examined. Additionally, by employing Lyapunov functions, the asymptotic stability—both local and global—of the equilibrium states is analyzed. Hyers-Ulam stability is also investigated.

A crucial aspect of diabetes management involves strategies based on parameter sensitivity, particularly concerning insulin injections and pharmaceutical interventions. By identifying key influential parameters, glucose regulation can be optimized. To extend model (1.1) to account for random perturbations, we incorporate stochastic terms as follows:

$$\begin{aligned} \mathscr{D}_t^{\nu}\mathtt{X}(t) &= \mathtt{X}_{in} - a\mathtt{X} - b\mathtt{X}\mathtt{Y} + \sigma_1\Psi_1(\mathtt{X},t)\,\dot{\mathrm{W}}_1, \\ \mathscr{D}_t^{\nu}\mathtt{Y}(t) &= \mathtt{Y}_{in} + c\mathtt{X} - \frac{d\,\mathtt{Y}}{e+\mathtt{Y}} + \sigma_2\Psi_2(\mathtt{Y},t)\,\dot{\mathrm{W}}_2. \end{aligned} \tag{1.3}$$

Here, $\mathrm{W}_i, (i = 1, 2)$ represent Brownian motion processes. The parameters $\sigma_i, (i = 1, 2)$ quantify noise intensity, while $\Psi_1(\mathtt{X}, t)$ and $\Psi_2(\mathtt{Y}, t)$ are stochastic constants. The diffusion coefficients are denoted as σ_1 and σ_2 for each state variable.

To solve the deterministic system, the fractional Predictor-Evaluator-Corrector-Evaluator (PECE) method based on the Adams-Bashforth-Moulton approach is utilized. The stochastic fractional diabetes model is handled using a fourth-order stochastic Runge-Kutta scheme, which is particularly effective for biological systems due to its stability, computational efficiency, and precision.

This study introduces an innovative fractional glucose-insulin model to overcome limitations in existing models. The incorporation of the Michaelis-Menten function, coupled with advanced numerical schemes, enhances the accuracy and applicability of the model in clinical environments, providing improved strategies for diabetes management.

Compared to fractional, ordinary, and partial differential equations, stochastic differential equations [37–44] are more effective in capturing realistic biological variability. Stochastic differential equations have also been employed in modeling infectious diseases, including COVID-19. Various mathematical frameworks, such as space-time, stochastic, fractional, and fractal models, have been utilized in epidemiological studies [46–49]. These methodologies help assess intervention strategies like social distancing and contact tracing.

Mathematical modeling is integral to public health decision-making, as it facilitates understanding of disease transmission dynamics and intervention outcomes. Simulating different outbreak scenarios assists policymakers in formulating effective strategies, optimizing resource allocation, and mitigating disease spread—an especially critical factor during pandemics where timely, data-driven decisions can save lives and reduce healthcare system burdens.

Understanding the complex interplay between glucose and insulin is crucial for effective diabetes management. Glucose, derived from carbohydrates in food sources such as grains, dairy, and meat, serves as a primary energy source for cells. While certain tissues, such as the brain, rely on insulin for glucose uptake, others, including muscle tissues, can absorb glucose independently. The pancreas plays a central role in glucose regulation by secreting insulin, a hormone that facilitates glucose metabolism and ensures stable energy availability.

Traditional glucose-insulin models often assume a linear insulin clearance rate, which may oversimplify the underlying physiological processes. However, experimental evidence suggests that insulin degradation follows a nonlinear mechanism better represented by the Michaelis-Menten function. This nonlinear approach provides a more accurate depiction of insulin dynamics, particularly in cases where excess insulin does not indefinitely accelerate its clearance. Building on this understanding, our study introduces a fractional-order stochastic glucose-insulin model that incorporates the Michaelis-Menten function to describe insulin degradation more realistically.

Moreover, the inherent variability and unpredictability in glucose metabolism necessitate the inclusion of stochasticity in mathematical models. Real-world biological systems, especially those influenced by external factors such as diet, exercise, and medication adherence, exhibit random fluctuations that cannot be fully captured by deterministic models. To address this, we extend our model by incorporating stochastic perturbations, allowing for a more realistic simulation of glucose-insulin dynamics under uncertain conditions.

To validate our analytical findings, we utilize numerical simulations based on the fractional predictor-corrector PECE method of Adams-Bashforth-Moulton type. Additionally, we employ the stochastic Runge-Kutta method of type 4, which enhances computational efficiency and accuracy in solving fractional stochastic differential equations. Sensitivity analysis is performed to identify key parameters affecting glucose regulation, leading to the development of optimized control strategies,

including insulin injections and pharmaceutical interventions.

This study contributes to the growing body of research on fractional stochastic modeling of diabetes by providing a robust framework for understanding glucose-insulin dynamics. The integration of fractional calculus and stochastic analysis offers new insights into diabetes progression and treatment, paving the way for improved disease management strategies and personalized therapeutic interventions.

The primary motivation of this work is to develop a more realistic and comprehensive mathematical framework for glucose-insulin regulation by incorporating two critical aspects: (1) the nonlinear insulin degradation described by the Michaelis-Menten function, which more accurately reflects physiological saturation effects, and (2) the inherent randomness and memory effects in biological systems, captured via stochastic fractional differential equations. The originality of this paper lies in the novel integration of Michaelis-Menten kinetics into a fractional stochastic glucose-insulin model—a combination that, to the best of our knowledge, has not been studied before. We provide a rigorous analysis of the model, including existence, uniqueness, boundedness, nonnegativity, and stability properties. Furthermore, we propose and numerically validate several control strategies based on parameter sensitivity, offering direct implications for personalized diabetes management.

In recent years, various fractional derivatives have been proposed, such as the local fractional derivative [50], He's fractional derivative [51], Atangana-Baleanu fractional derivative [52], M-truncated derivative [53], conformable fractional derivative [54], and Caputo β-derivative [55]. Each has distinct advantages: the local fractional derivative is effective on fractal sets, the Atangana-Baleanu derivative employs a non-singular kernel, and the conformable derivative obeys classical calculus rules. However, the Caputo derivative is chosen here because of its well-established theory, compatibility with standard initial conditions, and widespread adoption in biological modeling. Unlike the Riemann-Liouville derivative, the Caputo derivative of a constant is zero, making it suitable for systems with constant inputs or steady states. Its physical interpretation as a memory effect—where the rate of change depends on the entire history of the function—aligns with the long-term memory observed in glucose-insulin dynamics. While other derivatives may be explored in future extensions, the Caputo derivative provides a robust and interpretable foundation for this study.

Recent advances in fractional calculus have demonstrated its utility across diverse fields. For instance, exact wave solutions of the local fractional Vakhnenko-Parkes equation [56] illustrate how non-local operators describe wave propagation in fractal media. Similarly, the analysis of fractal active low-pass filters using local fractional derivatives on Cantor sets [57] highlights applications in engineering. In contrast, our work applies the Caputo derivative to a biomedical system, emphasizing its ability to model memory effects in physiological processes. While the aforementioned studies focus on exact solutions and circuit design, our contribution lies in developing a stochastic fractional model for a complex endocrine system, with direct implications for disease management. This comparative perspective underscores the versatility of fractional calculus and positions our work within the broader landscape of applied fractional modeling.

Recent studies on stability in fractional-order and stochastic systems provide a strong foundation for our analysis. For instance, the finite-time and global Mittag-Leffler stability of fractional-order neural networks with distributed delays [58], and the stochastic asymptotic stability for stochastic inertial Cohen-Grossberg neural networks with time-varying delays [59, 60] have been established. These

works highlight the importance of stability analysis in complex fractional stochastic systems, which motivates our investigation of the stability properties of the fractional stochastic glucose-insulin model.

The remainder of this paper is organized as follows. In Section 2, we present the fractional model and establish its fundamental properties, including existence, uniqueness, boundedness, and nonnegativity of solutions. Section 3 provides a detailed stability analysis, covering both asymptotic and Hyers-Ulam stability. Section 4 introduces four clinically-relevant control strategies for glucose regulation based on parameter sensitivity. In Section 5, we describe the numerical methods employed, including the fractional Adams-Bashforth-Moulton predictor-corrector scheme and the stochastic Runge-Kutta method, along with their convergence and validation. Section 6 presents and discusses the simulation results, comparing deterministic and stochastic dynamics. Finally, Section 7 discusses the implications of our findings, and Section 8 concludes the paper with remarks on applications and future work.

2. Solution properties

The Euler gamma function is given by

$$\Gamma(\nu) = \int_0^\infty e^{-t} t^{\nu-1} dt.$$

For a function $\psi(t) : \mathbb{R}^+ \to \mathbb{R}$, its fractional integral operator of order $\nu \in \mathbb{R}^+$ for $t > 0$ is defined as

$$I^\nu \psi(t) = \frac{1}{\Gamma(\nu)} \int_0^t (t-\sigma)^{\nu-1} \psi(\sigma) d\sigma.$$

As stated in [37], the Caputo fractional derivative of order $\nu > 0$, where $n - 1 < \nu < n$ and $n \in \mathbb{N}$, is formulated as

$${}_0^C\mathscr{D}_t^\nu \psi(t) = \begin{cases} \frac{1}{\Gamma(n-\nu)} \int_0^t \frac{\psi^{(n)}(\sigma)}{(t-\sigma)^{\nu+1-n}} d\sigma, & n-1 < \nu < n, \\ \frac{d^n}{dt^n}\psi(t), & \nu = n. \end{cases}$$

2.1. Existence and uniqueness

Setting

$$\Omega = \{(\mathtt{X}, \mathtt{Y}) \in \mathbb{R}^2 : \ \max(|\mathtt{X}|, |\mathtt{Y}|) \le \zeta\}.$$

Theorem 2.1. *Let $\dot{X}_0 = (\mathtt{X}_0, \mathtt{Y}_0) \in \Omega$ be an initial condition. A unique solution $\dot{X}(\mathtt{t}) \in \Omega$ of system (1.2) exists.*

Proof. For $\dot{X}, \overline{\dot{X}} \in \Omega$, suppose a mapping $T(\dot{X}) = (T_1(\dot{X}), T_2(\dot{X}))$ is defined as follows:

$$T_1(\dot{X}) = \mathtt{X}_{in} - a\mathtt{X} - b\mathtt{XY},$$
$$T_2(\dot{X}) = \mathtt{Y}_{in} + c\mathtt{X} - \frac{d\,\mathtt{Y}}{e + \mathtt{Y}}.$$

Thus

$$\begin{aligned} ||T(\dot{X}) - T(\overline{\dot{X}})|| &= |(a-b)\mathtt{Y}(\mathtt{X} - \mathring{\mathtt{X}})| + \Big|\frac{d\,\mathtt{Y}}{e+\mathtt{Y}} - \frac{d\,\mathring{\mathtt{Y}}}{e+\mathring{\mathtt{Y}}}\Big| \\ &\le (a - b\zeta)|\mathtt{X} - \mathring{\mathtt{X}}| + \Big(\frac{d}{e+\zeta}\Big)|\mathtt{Y} - \mathring{\mathtt{Y}}| \\ &\le \Gamma||\dot{X} - \overline{\dot{X}}||, \end{aligned}$$

where

$$\Gamma = \max\left\{(a - b\zeta), \left(\frac{d}{e+\zeta}\right)\right\}.$$

Thus, $T(\dot{X})$ satisfies the Lipschitz condition. The solutions to model (1.1) are unique and exist. □

2.2. Positivity and boundedness

Theorem 2.2. *(Positivity) If the initial conditions satisfy* $\mathtt{X}(0) \geq 0$ *and* $\mathtt{Y}(0) \geq 0$*, and all parameters* $\mathtt{X}_{\text{in}}, \mathtt{Y}_{\text{in}}, a, b, c, d, e$ *are nonnegative, then the solutions* $\mathtt{X}(t)$ *and* $\mathtt{Y}(t)$ *of system (1.2) remain nonnegative for all* $t \geq 0$*.*

Proof. Evaluating the fractional derivatives at the boundaries:

$$\mathscr{D}_t^{\nu}\mathtt{X}\Big|_{\mathtt{X}=0} = \mathtt{X}_{\text{in}} \geq 0, \qquad \mathscr{D}_t^{\nu}\mathtt{Y}\Big|_{\mathtt{Y}=0} = \mathtt{Y}_{\text{in}} + c\,\mathtt{X} \geq 0.$$

Since all parameters are nonnegative and $\mathtt{X}(t) \geq 0$, the result follows from the lemma in [34]. □

Theorem 2.3. *Model (1.2) solutions exhibit uniform boundedness in the positive region of* $\mathbb{R}^3_+$*,*

$$\Omega = \left\{(\mathtt{X}, \mathtt{Y}) \in \mathbb{R}^3_+ : N' \leq \frac{\mathtt{X}_{in} + \mathtt{Y}_{in}}{\varrho_1} + \nu, \quad \nu > 0\right\}.$$

Proof. As in [36] with $N' = x + y$, one obtains

$$\begin{aligned}
\mathscr{D}_t^{\nu}N' &= \mathtt{X}_{in} - a\mathtt{X} - b\mathtt{X}\mathtt{Y} + \mathtt{Y}_{in} + c\mathtt{X} - \frac{d\mathtt{Y}}{e + \mathtt{Y}} \\
&\leqslant \mathtt{X}_{in} + \mathtt{Y}_{in} - (a - c)\mathtt{X} - \frac{d\mathtt{Y}}{e + \mathscr{M}} \\
&\leqslant \mathtt{X}_{in} + \mathtt{Y}_{in} - \beta N(t),
\end{aligned}$$

where $\varrho_1 = \min\left\{a - c, \frac{d}{e+\mathscr{M}}\right\}$. For $\beta > 0$,

$$\mathscr{D}_t^{\nu}N' + \beta N' \leq \mathtt{X}_{in} + \mathtt{Y}_{in}.$$

Thus, [33] yields

$$0 \leq N' \leq N'(0)E_{\nu}(-\beta^{\nu}) + r^{\nu}E_{\nu,\nu+1}(-\beta^{\nu})).$$

Based on [34],

$$0 \leq N' \leq \frac{\mathtt{X}_{in} + \mathtt{Y}_{in}}{\beta}, \quad t \longrightarrow \infty.$$

For this model (1.2), the solution is uniformly bounded in Ω. □

2.3. Physical interpretation of the Caputo fractional derivative

The Caputo fractional derivative, defined in (2.1), is employed here to capture memory and hereditary properties in glucose-insulin dynamics. Physically, the derivative $\mathscr{D}_t^{\nu}\psi(t)$ represents a weighted accumulation of past changes, where the kernel $(t - \sigma)^{\nu-1}$ assigns greater weight to recent events. In physiological terms, this means that the current rate of change in glucose or insulin

concentration depends not only on the present state but also on the entire history of metabolic activity. This memory effect is particularly relevant in diabetes, where prolonged hyperglycemia can lead to irreversible tissue damage (glycemic memory). The Caputo formulation is preferred over other fractional derivatives because it allows initial conditions to be expressed in terms of integer-order derivatives, which are more readily measured and interpreted in clinical settings. Moreover, the Caputo derivative of a constant is zero, ensuring that constant inputs (e.g., basal insulin infusion) do not artificially induce spurious dynamics.

3. The stability of equilibrium

Theorem 3.1. *When $d > \mathtt{Y}_{in}$, the positive equilibrium $(\mathtt{X}^*, \mathtt{Y}^*)$ of system (1.2) is local asymptotically stable.*

Proof. For model (1.2), the Jacobian matrix $J(\mathtt{X}^*, \mathtt{Y}^*)$ at $(\mathtt{X}^*, \mathtt{Y}^*)$ is

$$J(\mathtt{X}^*, \mathtt{Y}^*) = \begin{pmatrix} -a - b\mathtt{Y}^* & -b\mathtt{X}^* \\ c & -\frac{de}{(e+\mathtt{Y}^*)^2} \end{pmatrix}.$$

Its characteristic equation:

$$\begin{aligned} |\lambda E - D|_{(\mathtt{X}^*,\mathtt{Y}^*)} &= (\lambda + a + b\mathtt{Y}^*)\left(\lambda + \frac{de}{(e+\mathtt{Y}^*)^2}\right) + cb\mathtt{X}^* \\ &= \lambda^2 + \left(a + b\mathtt{Y}^* + \frac{de}{(e+\mathtt{Y}^*)^2}\right)\lambda + (a + b\mathtt{Y}^*)\frac{de}{(e+\mathtt{Y}^*)^2} + cb\mathtt{X}^* \\ &= 0, \end{aligned}$$

then

$$\lambda_{1,2} = \frac{-\left(a + b\mathtt{Y}^* + \frac{de}{(e+\mathtt{Y}^*)^2}\right) \pm \sqrt{\left(a + b\mathtt{Y}^* + \frac{de}{(e+\mathtt{Y}^*)^2}\right)^2 - 4\left((a + b\mathtt{Y}^*)\frac{de}{(e+\mathtt{Y}^*)^2} + bc\mathtt{X}^*\right)}}{2}.$$

By analyzing the system's characteristic equation, we can determine the roots by solving for the eigenvalues. If the real parts of these eigenvalues are negative, the system is stable, and any perturbations will decay over time. Using the Routh-Hurwitz criterion, $(\mathtt{X}^*, \mathtt{Y}^*)$ is locally asymptotically stable if $d > \mathtt{Y}_{in}$. □

Theorem 3.2. *If $d > \mathtt{Y}_{in}$, then $(\mathtt{X}^*, \mathtt{Y}^*)$ of model (1.2) is global asymptotically stable.*

Proof. A Lyapunov function can be constructed to prove this:

$$\mathtt{L}(\mathtt{t}) = \frac{c}{2}(\mathtt{X} - \mathtt{X}^*)^2 + \frac{b\mathtt{X}^*}{2}(\mathtt{Y} - \mathtt{Y}^*)^2.$$

With respect to $\mathtt{t}$, L has fractional derivative

$$\begin{aligned}
\mathscr{D}_t^{\nu}\mathtt{L} &= c\,(\mathtt{X}-\mathtt{X}^*)\,\mathscr{D}_t^{\nu}\mathtt{X} + b\mathtt{X}^*\,(\mathtt{Y}-\mathtt{Y}^*)\,\mathscr{D}_t^{\nu}\mathtt{Y}\\
&= c\,(\mathtt{X}-\mathtt{X}^*)\,(\mathtt{X}_{in}-a\mathtt{X}-b\mathtt{X}\mathtt{Y}) + b\mathtt{X}^*\,(\mathtt{Y}-\mathtt{Y}^*)\left(\mathtt{Y}_{in}+c\mathtt{X}-\frac{d\mathtt{Y}}{e+\mathtt{Y}}\right)\\
&= c\,(\mathtt{X}-\mathtt{X}^*)\,(a\,(\mathtt{X}^*-\mathtt{X}) + b\,(\mathtt{X}^*\mathtt{Y}^*-\mathtt{X}\mathtt{Y}) + b\mathtt{X}^*\,(\mathtt{Y}-\mathtt{Y}^*)\left(c\,(\mathtt{X}-\mathtt{X}^*)-\frac{de\,(\mathtt{Y}^*-\mathtt{Y})}{(e+\mathtt{Y})\,(e+\mathtt{Y}^*)}\right)\\
&= -ac\,(\mathtt{X}-\mathtt{X}^*)^2 - bc\mathtt{Y}\,(\mathtt{X}-\mathtt{X}^*)^2 - \frac{bde\mathtt{X}^*\,(\mathtt{Y}-\mathtt{Y}^*)^2}{(e+\mathtt{Y})\,(e+\mathtt{Y}^*)}\\
&\leq 0.
\end{aligned}$$

Therefore, $\mathscr{D}_t^{\nu}\mathtt{L} \leq 0$. In addition, $\{(\mathtt{X},\mathtt{Y}) \in \Omega : \ \mathscr{D}_t^{\nu}\mathtt{L} = 0\}$ is the largest invariant set. Thus, using the invariance principle of LaSalle [35], $(\mathtt{X}^*,\mathtt{Y}^*)$ is asymptotically stable globally. It is obvious that $\mathscr{D}_t^{\nu}\mathtt{L} = 0$ holds if, and only if, $\mathtt{X} = \mathtt{X}^*$ and $\mathtt{Y} = \mathtt{Y}^*$, then the proof follows. □

Definition 3.1. *[61, 62] Assume that*

$$\begin{aligned}
\mathscr{W}_1(t,\mathtt{X}) &= \mathtt{X}_{in} - a\mathtt{X} - b\mathtt{X}\mathtt{Y},\\
\mathscr{W}_2(t,\mathtt{Y})) &= \mathtt{Y}_{in} + c\mathtt{X} - \frac{d\,\mathtt{Y}}{e+\mathtt{Y}}.
\end{aligned} \tag{3.1}$$

System (1.2) is Hyers-Ulam stable if $v_j > 0$ for $i \in N_j^2$, satisfying for every $\rho_j, i \in N_j^2$

$$\begin{aligned}
\left|\mathtt{X}(\mathtt{t}) - \frac{1}{\Gamma(\varrho_1)}\int_0^t (\mathtt{t}-\sigma)^{\varrho_1-1}\mathscr{W}_1(\sigma,\mathtt{X}(\sigma))d\sigma\right| &\leq \rho_1,\\
\left|\mathtt{Y}(\mathtt{t}) - \frac{1}{\Gamma(\varrho_1)}\int_0^t (\mathtt{t}-\sigma)^{\varrho_1-1}\mathscr{W}_2(\sigma,\mathtt{Y}(\sigma))d\sigma\right| &\leq \rho_2.
\end{aligned}$$

There is another solution $\left(\mathring{\mathtt{X}}(\mathtt{t}),\mathring{\mathtt{Y}}(\mathtt{t})\right)$ to the model (1.2). These solutions can be described using integral equations that fulfill their requirements.

$$\begin{aligned}
\mathring{\mathtt{X}}(\mathtt{t}) &= \frac{1}{\Gamma(\varrho_1)}\int_0^t (\mathtt{t}-\sigma)^{\varrho_1-1}\mathscr{W}_1\left(\sigma,\mathring{\mathtt{X}}(\sigma)\right)d\sigma,\\
\mathring{\mathtt{Y}}(\mathtt{t}) &= \frac{1}{\Gamma(\varrho_1)}\int_0^t (\mathtt{t}-\sigma)^{\varrho_1-1}\mathscr{W}_2\left(\sigma,\mathring{\mathtt{Y}}(\sigma)\right)d\sigma,
\end{aligned}$$

so that

$$\begin{aligned}
\left|\mathtt{X}(\mathtt{t}) - \mathring{\mathtt{X}}(\mathtt{t})\right| &\leq \phi_1\rho_1,\\
\left|\mathtt{Y}(\mathtt{t}) - \mathring{\mathtt{Y}}(\mathtt{t})\right| &\leq \phi_2\rho_2.
\end{aligned} \tag{3.2}$$

Theorem 3.3. *If (3.2) is true, then model (1.2) satisfies the Hyers-Ulam stability condition.*

Proof. According to Theorem 4,

$$\begin{aligned}
\left|\mathtt{X}(\mathtt{t}) - \mathring{\mathtt{X}}(\mathtt{t})\right| &= \frac{1}{\Gamma(\varrho_1)}\int_0^t (\mathtt{t}-\sigma)^{\varrho_1-1}\left(\mathscr{W}_1(\sigma,\mathtt{X}(\sigma)) - \mathscr{W}_1\left(\sigma,\mathring{\mathtt{X}}(\sigma)\right)\right)d\sigma\\
&\leq \frac{1}{\Gamma(\varrho_1)}\int_0^t (\mathtt{t}-\sigma)^{\varrho_1-1}\varrho_1\left\|\mathtt{X}-\mathring{\mathtt{X}}\right\|d\sigma\\
&\leq \varrho_1\left\|\mathtt{X}-\mathring{\mathtt{X}}\right\|.
\end{aligned}$$

Now, let $\left\|\mathtt{X}-\mathring{\mathtt{X}}\right\| = \phi_1$. Then

$$\left|\mathtt{X}(\mathtt{t})-\mathring{\mathtt{X}}(\mathtt{t})\right| \leq \phi_1\rho_1.$$

Similarly

$$\left|\mathtt{Y}(\mathtt{t})-\mathring{\mathtt{Y}}(\mathtt{t})\right| \leq \phi_2\rho_2,$$

with $\left\|\mathtt{Y}-\mathring{\mathtt{Y}}\right\| = \phi_2$. □

4. Strategies to control glucose levels

A combined approach involving simultaneous adjustments to b, c, and d can provide a more holistic management strategy for controlling glucose levels. By synergistically enhancing insulin sensitivity, reducing glucose production, and prolonging insulin action, this strategy aims to maintain glucose levels within the normal range. This applies both during fasting and postprandial periods. By adjusting certain parameters, we propose clinically applicable treatments for controlling glucose levels ($\mathtt{X}$). Since patients with diabetes typically exhibit higher plasma glucose levels, it is advisable to reduce carbohydrate intake, thereby decreasing the ratio $\mathtt{X}_{in}$. Instead of focusing on the insulin-independent utilization rate a, we concentrate on other parameters: b, c, and d. We keep a at a constant value. Glucose levels are significantly influenced by insulin, so our analysis will always follow the WHO's recommended blood glucose levels: a normal fasting glucose range is $70 < \mathtt{X} < 110$ mg/dl and below 140 mg/dl two hours postprandial. The parameters used are derived from references [5], with the necessary unit conversions applied. We propose four specific strategies, each based on simulations, which demonstrate their potential effectiveness in controlling blood glucose levels according to WHO guidelines. The parameters and their units used in these strategies have been carefully selected and converted from the cited references [5] to ensure accurate and clinically relevant results.

4.1. Strategy 1: Adjusting parameter b

By fine-tuning parameter b, which influences the insulin sensitivity of glucose utilization, we can enhance the body's ability to lower blood glucose levels in response to insulin. This strategy targets improving insulin efficiency in glucose uptake, thereby reducing hyperglycemia. By improving the insulin resistance parameter b, we can further decrease the glucose level $\mathtt{X}^*$. This can be achieved by using metformin. With no insulin injection, we derive the relationship:

$$b = \frac{(x_{in} - a\mathtt{X}^*)(d - c\mathtt{X}^*)}{ceG^{*2}}.$$

Using the given values, we find:

$$b = \frac{(4.5 - 0.0002 \times 90)(1500 - 0.2298 \times 90)}{0.2298 \times 2300 \times 90^2} \approx 6.85 \times 10^{-6}.$$

Figure 1 shows the behavior of glucose $\mathtt{X}(t)$ and insulin $\mathtt{Y}(t)$ using $b = 7.5919e{-}4, 8.5919e{-}4, 9.5919e{-}4, 10.5919e-4$.

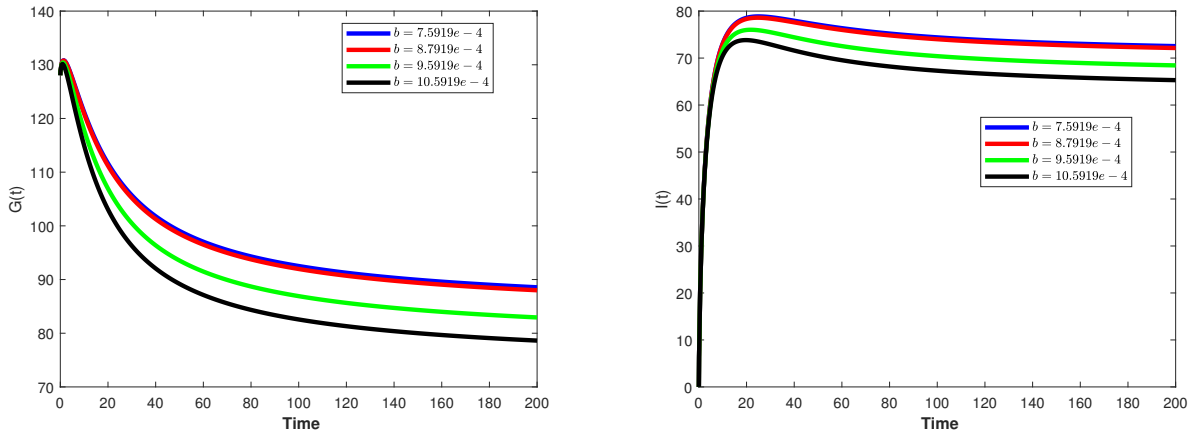

(a) Glucose concentration $\mathtt{X}(t)$ dynamics under varying values of b. (b) Insulin concentration $\mathtt{Y}(t)$ dynamics under varying values of b.

Figure 1. Behavior of glucose and insulin concentrations for $b = 7.5919 \times 10^{-4},\ 8.5919 \times 10^{-4},\ 9.5919 \times 10^{-4},\ 10.5919 \times 10^{-4}$: (a) Glucose $\mathtt{X}(t)$ response; (b) Insulin $\mathtt{Y}(t)$ response.

4.2. Strategy 2: Adjust insulin doses

For patients with Type 1 Diabetes Mellitus (T1DM), artificial insulin injections will be necessary for the rest of their lives due to damaged ν cells. Glucose is decomposed here. Insulin injections are also recommended for T2DM patients. First, we adjust the insulin dose to maintain glucose levels $\mathtt{X}^*$ within the normal range. Based on x_{in}, a, b, c, d, e, we can substitute $\mathtt{Y}_{in}$ into the second equation of (1.2) below:

$$\mathtt{Y}_{in} = \frac{d\frac{x_{in}-a\mathtt{X}^*}{b\mathtt{X}^*}}{e + \frac{x_{in}-a\mathtt{X}^*}{b\mathtt{X}^*}} - c\mathtt{X}^* = \frac{d(x_{in} - a\mathtt{X}^*)}{eb\mathtt{X}^* + (x_{in} - a\mathtt{X}^*)} - c\mathtt{X}^*.$$

The results indicate that $\mathtt{X}^*$ can be maintained within the normal range with an adjustment of injection dose (see Figure 2(a)). The profile shows that $\mathtt{X}^*$ decreases as the insulin dosage $\mathtt{Y}_{in}$ moves up. Diabetes patients' ν cells secrete insulin, but glucose cannot be broken down properly. In one case, secreted insulin is not enough; in another, insulin resistance occurs despite sufficient insulin levels. Under these conditions, we designed three strategies for T2DM without insulin injection.

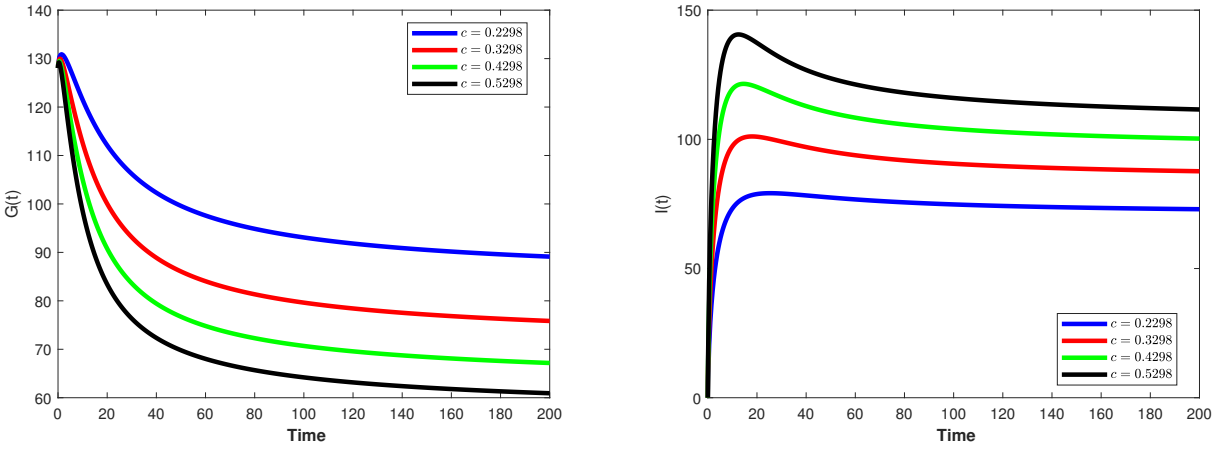

(a) Glucose concentration $\mathtt{X}(t)$ dynamics for varying values of c. (b) Insulin concentration $\mathtt{Y}(t)$ dynamics for varying values of c.

Figure 2. Dynamic behavior of the system for different values of the glucose production rate $c = 0.2298,\ 0.3298,\ 0.4298,\ 0.5298$: (a) Glucose concentration $\mathtt{X}(t)$; (b) Insulin concentration $\mathtt{Y}(t)$.

4.3. Strategy 3: Modifying parameter c

Parameter c represents the rate of glucose production. Reducing c can decrease endogenous glucose production, helping to lower overall blood glucose levels. This approach may be particularly beneficial for patients who have excessive hepatic glucose production. Stimulating insulin secretion increases the rate parameter c, which also helps control the glucose level $\mathtt{X}^*$. The relationship is given by:

$$c = \frac{d(x_{in} - a\mathtt{X}^*)}{\mathtt{X}^*(eb\mathtt{X}^* + x_{in} - a\mathtt{X}^*)}.$$

Using the given values, we find:

$$c = \frac{1500(4.5 - 0.0002 \times 90)}{90(2300 \times 7.5919 \times 10^{-4} \times 90 + 4.5 - 0.0002 \times 90)} \approx 0.2256.$$

Figure 2 shows the behavior of glucose $\mathtt{X}(t)$ and insulin $\mathtt{Y}(t)$ using $c = 0.2298, 0.3298, 0.4298, 0.5298$.

4.4. Strategy 4: Regulating parameter d

Parameter d affects the degradation rate of insulin. By optimizing d, we can prolong the insulin's effectiveness in the bloodstream, thereby enhancing its ability to manage postprandial glucose spikes. This strategy is crucial for maintaining glucose levels within the recommended postprandial range. Finally, we can control the glucose level by adjusting insulin clearance rate (d). As a result, $\mathtt{X}^* = \mathtt{X}/(1+d)$, where $\mathtt{X}$ is the initial glucose level. This equation shows that by lowering the insulin clearance rate, the glucose level can be managed more effectively.

$$d = \frac{c\mathtt{X}^*(be\mathtt{X}^* + \mathtt{X}_{in} - a\mathtt{X}^*)}{x_{in} - a\mathtt{X}^*}.$$

Using the given values, we find:

$$d = \frac{0.2298 \times 90 \times (7.5919 \times 10^{-4} \times 2300 \times 90 + 4.5 - 0.0002 \times 90)}{4.5 - 0.0002 \times 90} \approx 745.85.$$

By managing d, we ensure that $\mathtt{X}^*$ remains within the desired range, contributing to better glucose control in diabetic patients. Figure 3 shows the behavior of glucose $\mathtt{X}(t)$ and insulin $\mathtt{Y}(t)$ using $d = 745.85, 1000, 1200, 1500$.

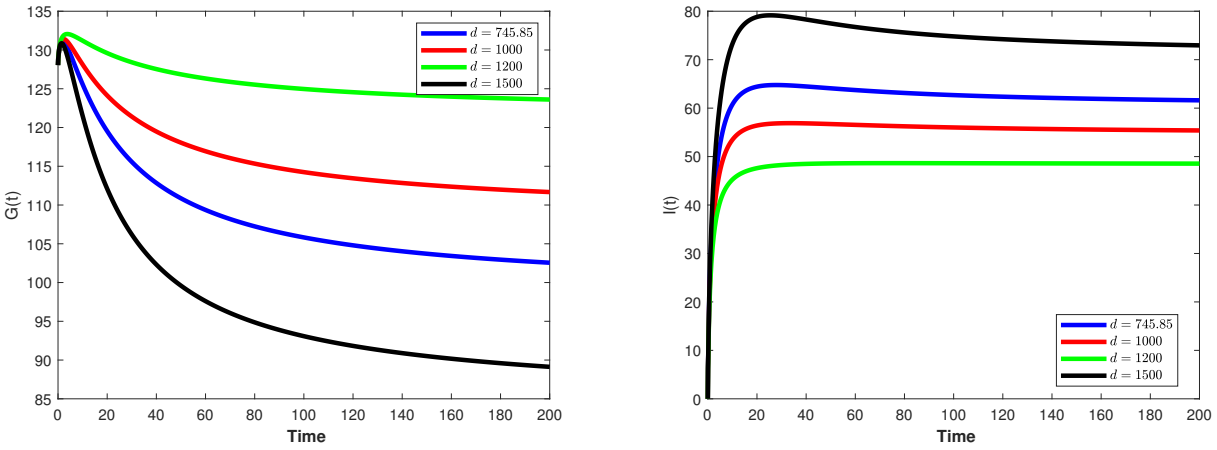

(a) Glucose concentration $\mathtt{X}(t)$ dynamics for varying values of d. (b) Insulin concentration $\mathtt{Y}(t)$ dynamics for varying values of d.

Figure 3. Dynamic behavior of the system for different values of the insulin clearance rate $d = 745.85,\ 1000,\ 1200,\ 1500$: (a) Glucose concentration $\mathtt{X}(t)$; (b) Insulin concentration $\mathtt{Y}(t)$.

In conclusion, by combining these strategies, we can achieve more comprehensive and effective management of glucose levels in diabetic patients. Each strategy targets a specific aspect of glucose-insulin dynamics, providing a tailored approach to diabetes treatment. By implementing these strategies in clinical practice, we can help patients maintain glucose levels within the recommended range, thereby improving their overall health and quality of life. Glucose levels are significantly influenced by insulin, so our analysis will always follow the WHO's recommended blood glucose levels: a normal fasting glucose range is $70 < \mathtt{X} < 110$ mg/dl and below 140 mg/dl two hours postprandial. Simulations in Figures 2 and 3 illustrate these adjustments.

5. Computing numerical techniques

5.1. Implementation of the fractional Adams-Bashforth-Moulton method

Diethelm et al. [63] performed the initial research on the fractional Adams method, which can be expressed as follows:

$$\mathtt{X}^p_{\mathrm{n}+1} = \sum_{j=0}^{k-1} \frac{t^j_{\mathrm{n}+1}}{j!} \mathtt{X}^{(j)}_0 + \hbar \sum_{j=0}^{n} \ell_{j,\mathrm{n}+1} f(t_j, \mathtt{X}_j),$$

$$\mathtt{X}_{\mathtt{n}+1} = \sum_{j=0}^{k-1} \frac{t_{\mathtt{n}+1}^{j}}{j!} \mathtt{Y}_0^{(j)} + \frac{h^{\nu}}{\Gamma(\nu+2)} \left(\sum_{j=0}^{n} \ell_{j,\mathtt{n}+1} f(t_j, \mathtt{X}_j) + \ell_{n+1,\mathtt{n}+1} f(t_{\mathtt{n}+1}, \mathtt{X}_{\mathtt{n}+1}^{p}) \right).$$

Here, the coefficients $\ell_{j,\mathtt{n}+1}$ are given by:

$$\ell_{j,\mathtt{n}+1} = \begin{cases} \mathtt{n}^{\nu+1} - (\mathtt{n}-\nu)(\mathtt{n}+1)^{\nu}, & \text{if } j = 0, \\ (\mathtt{n}-j+2)^{\nu+1} + (\mathtt{n}-j)^{\nu+1} - 2(\mathtt{n}-j+1)^{\nu+1}, & \text{if } 1 \le j \le n, \\ 1, & \text{if } j = \mathtt{n}+1. \end{cases}$$

Applying this scheme to the fractional-order system:

$$\begin{aligned} \mathscr{D}_t^{\nu} \mathtt{X}(t) &= \mathtt{X}_{in} - a\mathtt{X} - b\mathtt{X}\mathtt{Y}, \qquad \mathtt{X}(0) = \mathtt{X}_0, \\ \mathscr{D}_t^{\nu} \mathtt{Y}(t) &= \mathtt{Y}_{in} + c\mathtt{X} - \frac{d\,\mathtt{Y}}{e+\mathtt{Y}}, \qquad \mathtt{Y}(0) = \mathtt{Y}_0, \end{aligned}$$

we obtain the discrete form:

$$\begin{aligned} \mathtt{X}_{\mathtt{n}+1} &= \mathtt{X}_0 + \frac{h^{\nu}}{\Gamma(\nu+2)} \Big(\mathtt{X}_{i\mathtt{n}} - a\mathtt{X}_{\mathtt{n}+1}^{p} - b\mathtt{X}_{\mathtt{n}+1}^{p} \mathtt{Y}_{\mathtt{n}+1}^{p} \Big) \\ &\quad + \frac{h^{\nu}}{\Gamma(\nu+2)} \sum_{j=0}^{n} \Psi_{j,\mathtt{n}+1} \Big(\mathtt{X}_{i\mathtt{n}} - a\mathtt{X}(t_j) - b\mathtt{X}(t_j)\mathtt{Y}(t_j) \Big), \\ \mathtt{Y}_{\mathtt{n}+1} &= \mathtt{Y}_0 + \frac{h^{\nu}}{\Gamma(\nu+2)} \Big(\mathtt{Y}_{i\mathtt{n}} + c\mathtt{X}_{\mathtt{n}+1}^{p} - \frac{d\,\mathtt{Y}_{\mathtt{n}+1}^{p}}{e+\mathtt{Y}_{\mathtt{n}+1}^{p}} \Big) \\ &\quad + \frac{h^{\nu}}{\Gamma(\nu+2)} \sum_{j=0}^{n} \Psi_{j,\mathtt{n}+1} \Big(\mathtt{Y}_{i\mathtt{n}} + c\mathtt{X}(t_j) - \frac{d\,\mathtt{Y}(t_j)}{e+\mathtt{Y}(t_j)} \Big), \end{aligned}$$

where the predictor step is given by:

$$\begin{aligned} \mathtt{X}_{\mathtt{n}+1}^{p} &= \mathtt{X}_0 + \frac{h^{\nu}}{\Gamma(\nu+2)} \sum_{j=0}^{n} \Psi_{j,\mathtt{n}+1} \Big(\mathtt{X}_{i\mathtt{n}} - a\mathtt{X}(t_j) - b\mathtt{X}(t_j)\mathtt{Y}(t_j) \Big), \\ \mathtt{Y}_{\mathtt{n}+1}^{p} &= \mathtt{Y}_0 + \frac{h^{\nu}}{\Gamma(\nu+2)} \sum_{j=0}^{n} \Psi_{j,\mathtt{n}+1} \Big(\mathtt{Y}_{i\mathtt{n}} + c\mathtt{X}(t_j) - \frac{d\,\mathtt{Y}(t_j)}{e+\mathtt{Y}(t_j)} \Big). \end{aligned}$$

5.2. Numerical implementation via the Milstein scheme

We consider the stochastic counterpart of the glucose-insulin model

$$\begin{aligned} \mathscr{D}_t^{\nu} X(t) &= X_{\mathrm{in}} - aX - bXY, \\ \mathscr{D}_t^{\nu} Y(t) &= Y_{\mathrm{in}} + cX - \frac{d\,Y}{e+Y}, \end{aligned}$$

perturbed by multiplicative noise in each component. As in [64], in differential form, we write

$$\mathrm{d}X = f_1(X,Y)\,\mathrm{d}t + g_1(X)\,\mathrm{d}W_1, \qquad \mathrm{d}Y = f_2(X,Y)\,\mathrm{d}t + g_2(Y)\,\mathrm{d}W_2,$$

where

$$f_1(X, Y) = X_{\text{in}} - aX - bXY, \qquad f_2(X, Y) = Y_{\text{in}} + cX - \frac{d\,Y}{e + Y}.$$

We adopt multiplicative diffusion coefficients

$$g_1(X) = \sigma_X\, X, \qquad g_2(Y) = \sigma_Y\, Y,$$

with independent Wiener processes W_1 and W_2. To be consistent with the fractional order $\nu \in (0, 1]$, we follow the same step-scaling used in the Generalized Runge-Kutta method of type 4 (GRK4M) section and introduce

$$\hbar \;=\; \frac{h^\nu}{\Gamma(\nu + 1)},$$

while keeping the stochastic increments $\Delta W \sim \mathcal{N}(0, h)$ standard in time.

Let $t_n = nh$, and denote $(X_n, Y_n) \approx (X(t_n), Y(t_n))$. The Milstein updates read

$$X_{n+1} = X_n + f_1(X_n, Y_n)\,\hbar + g_1(X_n)\,\Delta W_1 + \tfrac{1}{2}\, g_1(X_n)\, g_1'(X_n)\,((\Delta W_1)^2 - h),$$
$$Y_{n+1} = Y_n + f_2(X_n, Y_n)\,\hbar + g_2(Y_n)\,\Delta W_2 + \tfrac{1}{2}\, g_2(Y_n)\, g_2'(Y_n)\,((\Delta W_2)^2 - h),$$

where $\Delta W_i \sim \mathcal{N}(0, h)$ are independent. For $g_1(X) = \sigma_X X$ and $g_2(Y) = \sigma_Y Y$ one has $g_1'(X) = \sigma_X$ and $g_2'(Y) = \sigma_Y$, hence

$$X_{n+1} = X_n + f_1(X_n, Y_n)\,\hbar + \sigma_X X_n\,\Delta W_1 + \tfrac{1}{2}\,\sigma_X^2 X_n\,((\Delta W_1)^2 - h),$$
$$Y_{n+1} = Y_n + f_2(X_n, Y_n)\,\hbar + \sigma_Y Y_n\,\Delta W_2 + \tfrac{1}{2}\,\sigma_Y^2 Y_n\,((\Delta W_2)^2 - h).$$

In practice we also enforce nonnegativity $X_{n+1} = \max\{X_{n+1}, 0\}$ and $Y_{n+1} = \max\{Y_{n+1}, 0\}$. We report ensemble means and 95% confidence intervals computed over N_{sim} sample paths and explore several noise intensities σ_X, σ_Y.

5.3. Justification and convergence of numerical methods

Choice of Runge-Kutta methods Although the RK method is not new, its selection in this work is motivated by several critical advantages: (1) RK methods are explicit and do not require solving nonlinear equations at each step, reducing computational cost; (2) the classical RK4 provides an excellent balance between accuracy and stability for deterministic systems; (3) for stochastic systems, the stochastic RK4 (SRK4) method extends these benefits to stochastic differential equations while maintaining strong convergence and numerical stability. The fractional Adams-Bashforth-Moulton (ABM) predictor-corrector method is used for the deterministic fractional system due to its proven convergence and ability to handle nonlocal fractional operators efficiently.

Convergence analysis The convergence of the fractional ABM method for Caputo fractional differential equations is well-established [63]. The method converges with order $O(h^p)$ where $p = \min\{2, 1 + \nu\}$ for $\nu > 0$. For the SRK4 method, under standard Lipschitz and growth conditions, strong convergence of order 1.0 and weak convergence of order 2.0 are guaranteed [64]. Numerical stability is ensured through step-size adaptation and consistency checks.

Limitations and validation The primary limitation of RK methods is their fixed-step nature, which may become inefficient for stiff systems. However, in our glucose-insulin model, stiffness is mitigated by appropriate parameter scaling. To validate the obtained solutions, we performed multiple checks: (1) comparison with known analytic solutions for simplified cases; (2) verification of nonnegativity and boundedness as established in Theorems 2 and 3; (3) sensitivity analysis to time-step size, confirming solution convergence as $h \to 0$; and (4) physiological plausibility checks against clinical data ranges.

6. Figure descriptions and analysis

6.1. Comparison between ABM and GRKM

Figures 4–11 show the behavior of the fractional deterministic diabetes mellitus model (1.2) for various fractional orders $\nu = 0.7$, $\nu = 0.75$, $\nu = 0.85$, $\nu = 0.95$, $\nu = 1$ at $\mathbf{Y}_{\text{in}} = 0, 5, 10, 20$.

Figures 4 and 5 illustrate the dynamics of $\mathbf{X}(t)$ and insulin levels, respectively, under the ABM method and the GRKM method for different values of ν with an insulin input of $\mathbf{Y}_{\text{in}} = 20$. These comparisons provide insight into how the two methods influence glucose and insulin regulation under the given conditions.

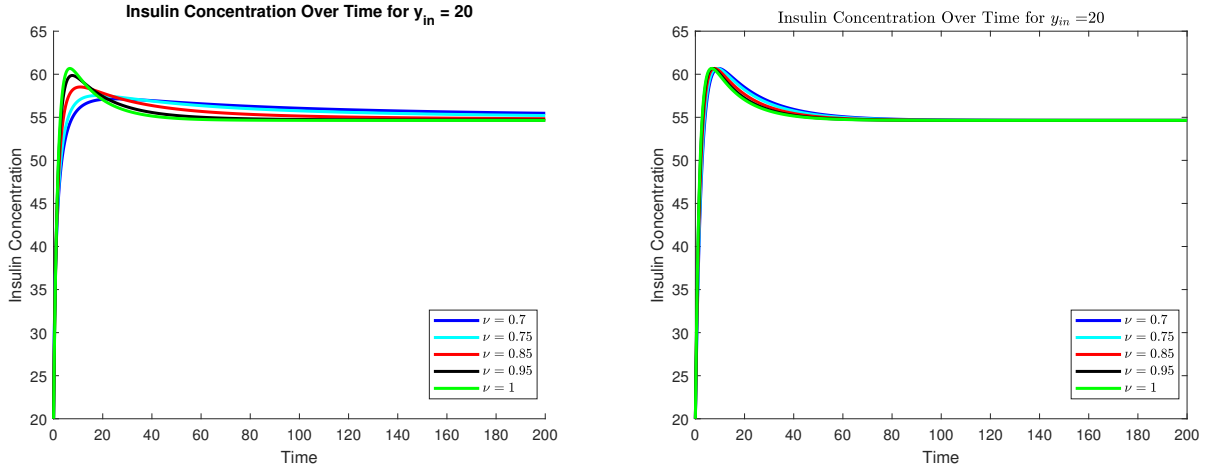

(a) ABM method: Glucose $\mathbf{X}(t)$ dynamics for fractional orders $\nu = 0.7, 0.75, 0.85, 0.95, 1$ at $\mathbf{Y}_{\text{in}} = 20$

(b) GRKM method: Glucose $\mathbf{X}(t)$ dynamics for fractional orders $\nu = 0.7, 0.75, 0.85, 0.95, 1$ at $\mathbf{Y}_{\text{in}} = 20$

Figure 4. Comparison of $\mathbf{X}(t)$ dynamics under ABM and GRKM at $\mathbf{Y}_{\text{in}} = 20$ for fractional orders $\nu = 0.7, 0.75, 0.85, 0.95, 1$. (a) ABM solution showing glucose decay with memory-dependent dynamics. (b) GRKM solution showing similar glucose decay with slightly different convergence properties.

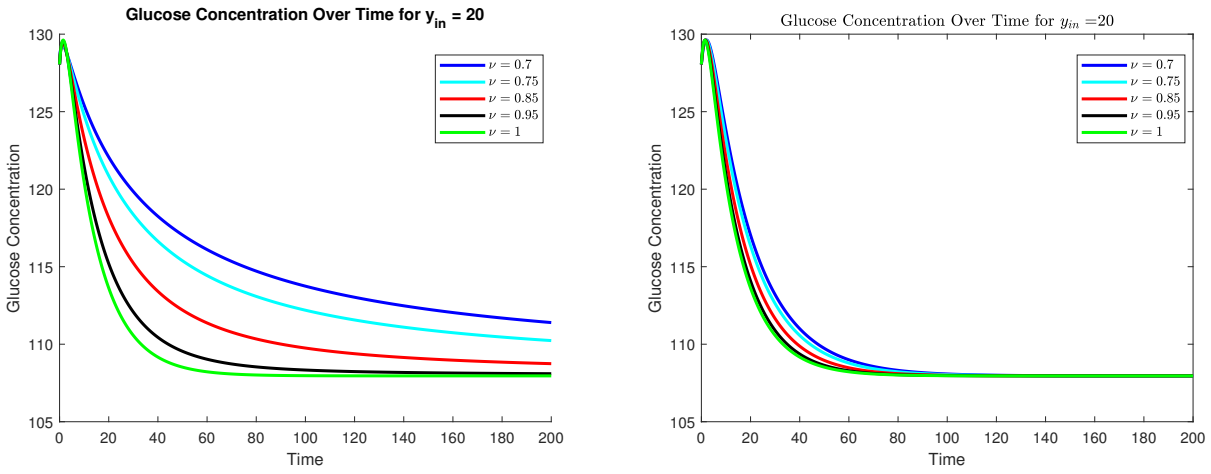

(a) ABM method: Insulin $\mathbf{Y}(t)$ dynamics for fractional orders $\nu = 0.7, 0.75, 0.85, 0.95, 1$ at $\mathbf{Y}_{\text{in}} = 20$

(b) GRKM method: Insulin $\mathbf{Y}(t)$ dynamics for fractional orders $\nu = 0.7, 0.75, 0.85, 0.95, 1$ at $\mathbf{Y}_{\text{in}} = 20$

Figure 5. Comparison of $\mathbf{Y}(t)$ dynamics under ABM and GRKM at $\mathbf{Y}_{\text{in}} = 20$ for fractional orders $\nu = 0.7, 0.75, 0.85, 0.95, 1$. (a) ABM solution showing insulin response to glucose with fractional memory effects. (b) GRKM solution showing insulin dynamics with faster stabilization.

Similarly, Figures 6 and 7 present the behavior of $\mathbf{X}(t)$ and insulin levels for $\mathbf{Y}_{\text{in}} = 10$. A comparison with Figures 4 and 5 suggest that glucose levels remain more elevated at $\mathbf{Y}_{\text{in}} = 10$ compared to $\mathbf{Y}_{\text{in}} = 20$, indicating a dose-dependent regulatory effect of insulin. This demonstrates that the system's response to insulin input varies proportionally with the administered dose.

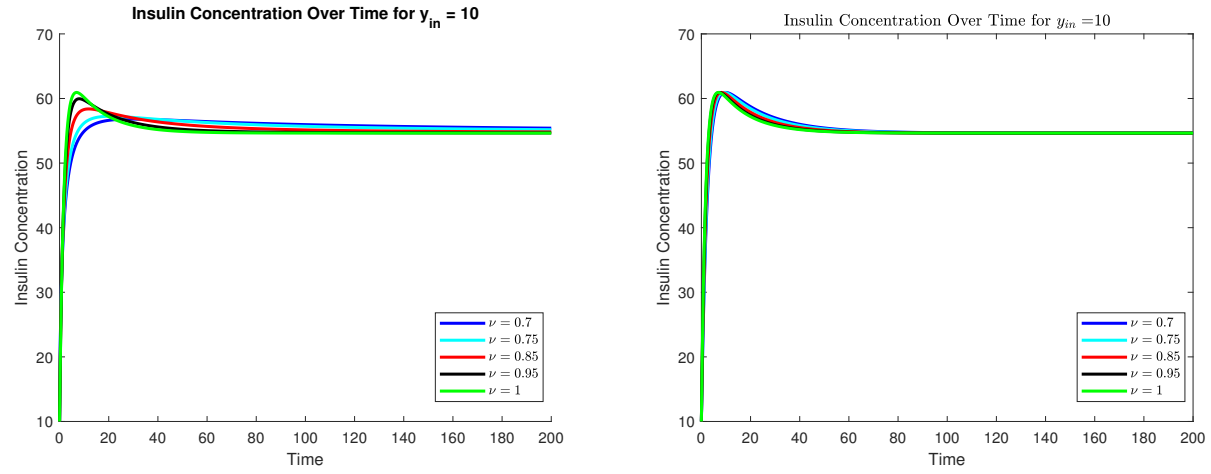

(a) ABM method: Glucose $\mathbf{X}(t)$ dynamics at $\mathbf{Y}_{\text{in}} = 10$ for fractional orders $\nu = 0.7, 0.75, 0.85, 0.95, 1$

(b) GRKM method: Glucose $\mathbf{X}(t)$ dynamics at $\mathbf{Y}_{\text{in}} = 10$ for fractional orders $\nu = 0.7, 0.75, 0.85, 0.95, 1$

Figure 6. Comparison of $\mathbf{X}(t)$ dynamics under ABM and GRKM at $\mathbf{Y}_{\text{in}} = 10$ for fractional orders $\nu = 0.7, 0.75, 0.85, 0.95, 1$. (a) ABM glucose trajectory showing slower decay due to reduced insulin input. (b) GRKM glucose trajectory with similar steady-state but different transient behavior.

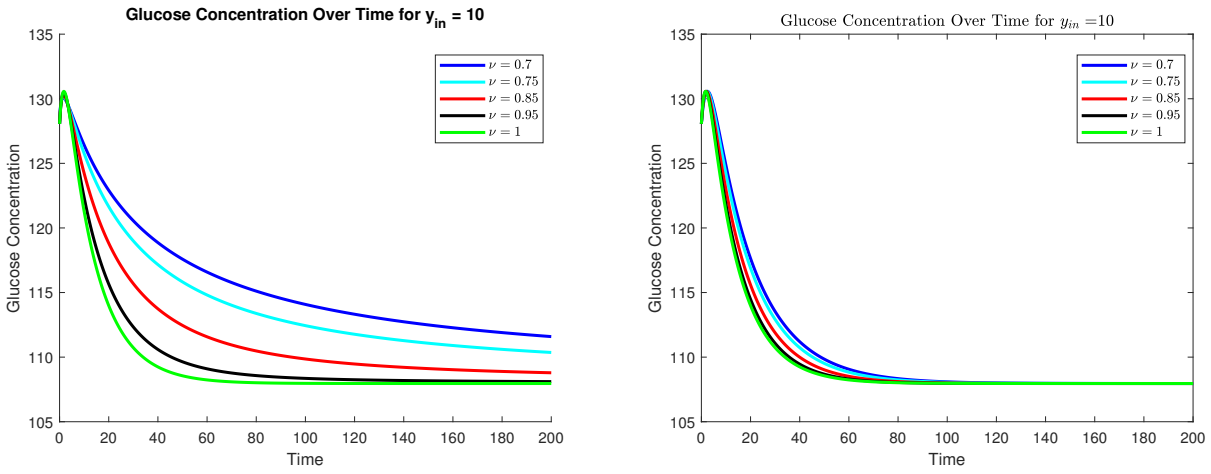

(a) ABM method: Insulin $\mathbf{Y}(t)$ dynamics at $\mathbf{Y}_{\text{in}} = 10$ for fractional orders $\nu = 0.7, 0.75, 0.85, 0.95, 1$

(b) GRKM method: Insulin $\mathbf{Y}(t)$ dynamics at $\mathbf{Y}_{\text{in}} = 10$ for fractional orders $\nu = 0.7, 0.75, 0.85, 0.95, 1$

Figure 7. Comparison of $\mathbf{Y}(t)$ dynamics under ABM and GRKM at $\mathbf{Y}_{\text{in}} = 10$ for fractional orders $\nu = 0.7, 0.75, 0.85, 0.95, 1$. (a) ABM insulin response with persistent memory effects. (b) GRKM insulin dynamics approaching equilibrium more rapidly.

Figures 8 and 9 further explore the system's response at a lower insulin input of $\mathbf{Y}_{\text{in}} = 5$, again comparing the ABM and GRKM models. The trends observed in these figures highlight how reducing insulin input results in progressively higher steady-state glucose levels and lower insulin concentrations, confirming the monotonic relationship between exogenous insulin and glycemic control.

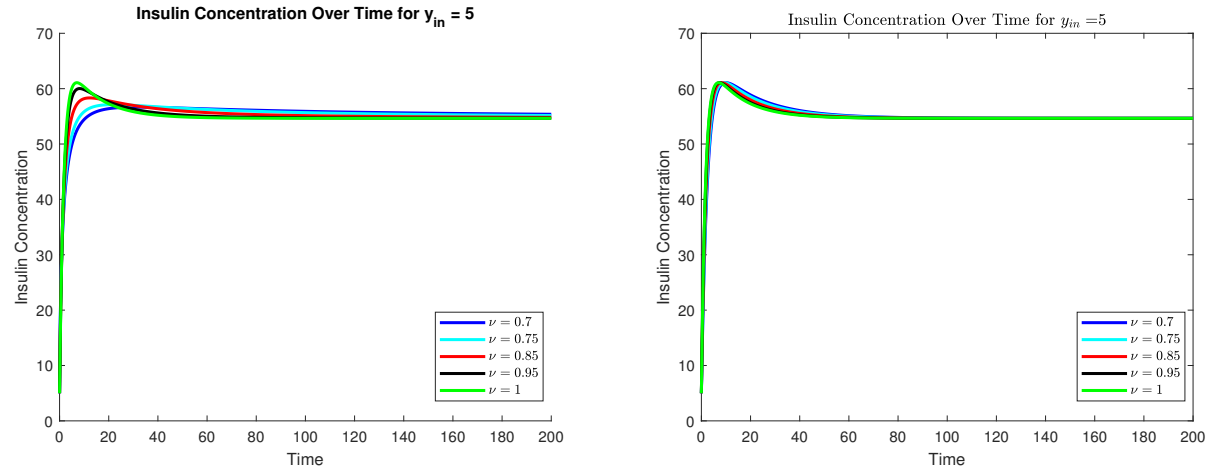

(a) ABM method: Glucose $\mathbf{X}(t)$ dynamics at $\mathbf{Y}_{\text{in}} = 5$ for fractional orders $\nu = 0.7, 0.75, 0.85, 0.95, 1$

(b) GRKM method: Glucose $\mathbf{X}(t)$ dynamics at $\mathbf{Y}_{\text{in}} = 5$ for fractional orders $\nu = 0.7, 0.75, 0.85, 0.95, 1$

Figure 8. Comparison of $\mathbf{X}(t)$ dynamics under ABM and GRKM at $\mathbf{Y}_{\text{in}} = 5$ for fractional orders $\nu = 0.7, 0.75, 0.85, 0.95, 1$. (a) ABM glucose elevation persists due to low exogenous insulin. (b) GRKM glucose shows similar patterns with numerical method variations.

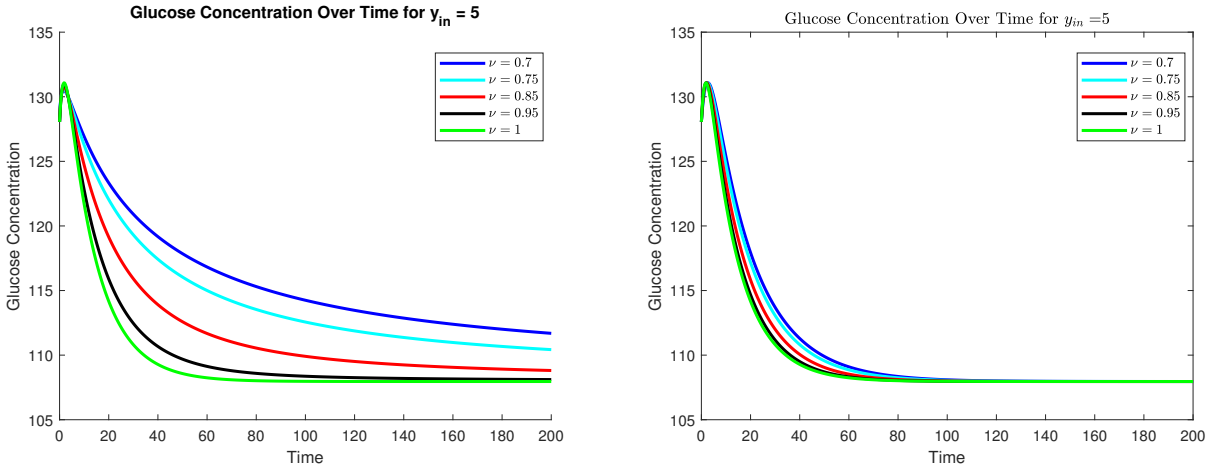

(a) ABM method: Insulin $\mathbf{Y}(t)$ dynamics at $\mathbf{Y}_{\text{in}} = 5$ for fractional orders $\nu = 0.7, 0.75, 0.85, 0.95, 1$

(b) GRKM method: Insulin $\mathbf{Y}(t)$ dynamics at $\mathbf{Y}_{\text{in}} = 5$ for fractional orders $\nu = 0.7, 0.75, 0.85, 0.95, 1$

Figure 9. Comparison of $\mathbf{Y}(t)$ dynamics under ABM and GRKM at $\mathbf{Y}_{\text{in}} = 5$ for fractional orders $\nu = 0.7, 0.75, 0.85, 0.95, 1$. (a) ABM insulin trajectory with reduced peak levels. (b) GRKM insulin showing consistent equilibrium attainment.

Additionally, Figures 10 and 11 provide the baseline case without exogenous insulin ($\mathbf{Y}_{\text{in}} = 0$), reinforcing the observed patterns in glucose-insulin dynamics. These figures demonstrate that endogenous insulin production alone is insufficient to maintain normoglycemia under the model parameters, consistent with diabetic pathophysiology.

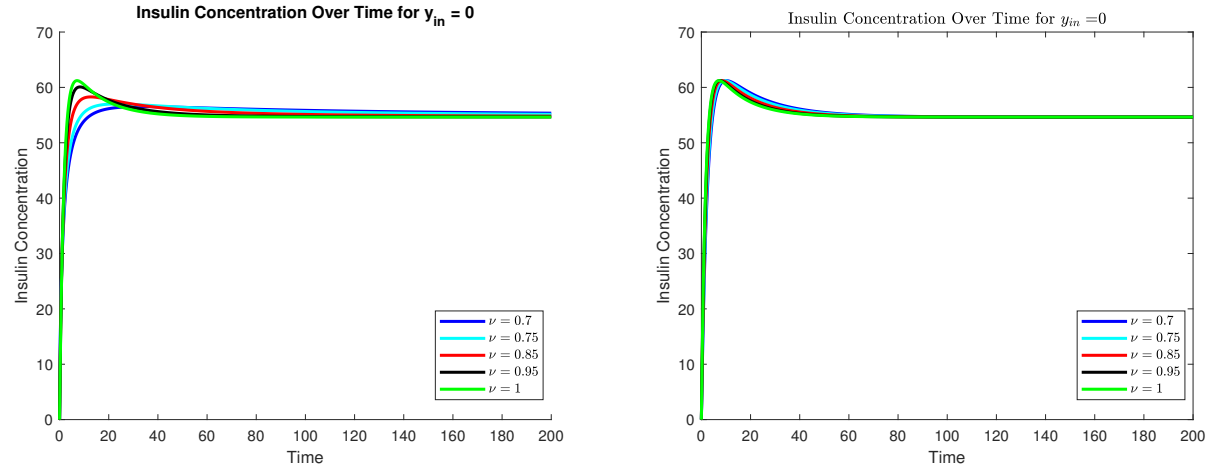

(a) ABM method: Glucose $\mathbf{X}(t)$ dynamics at $\mathbf{Y}_{\text{in}} = 0$ for fractional orders $\nu = 0.7, 0.75, 0.85, 0.95, 1$

(b) GRKM method: Glucose $\mathbf{X}(t)$ dynamics at $\mathbf{Y}_{\text{in}} = 0$ for fractional orders $\nu = 0.7, 0.75, 0.85, 0.95, 1$

Figure 10. Comparison of $\mathbf{X}(t)$ dynamics under ABM and GRKM at $\mathbf{Y}_{\text{in}} = 0$ for fractional orders $\nu = 0.7, 0.75, 0.85, 0.95, 1$. (a) ABM glucose remains elevated without exogenous insulin. (b) GRKM glucose shows similar hyperglycemic steady-state.

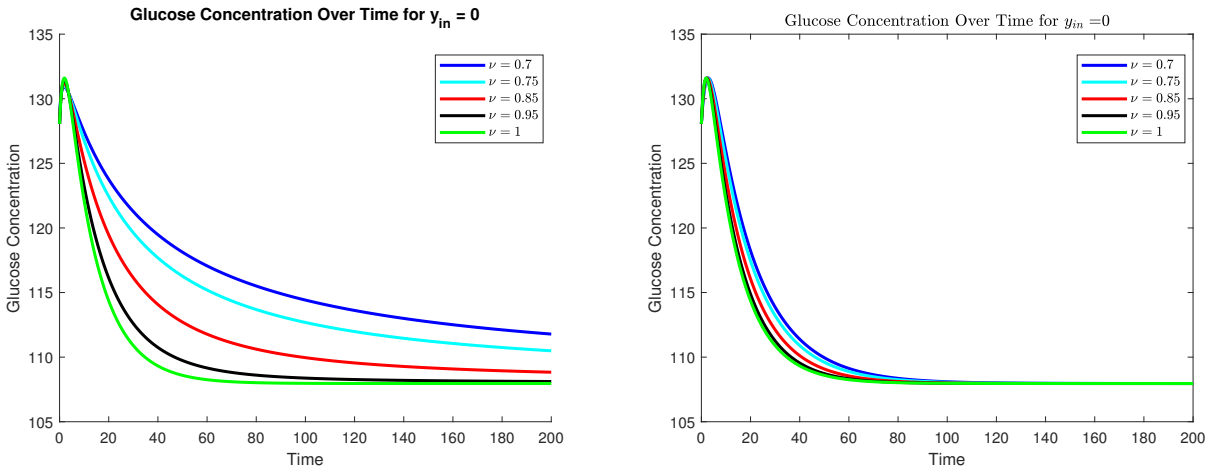

(a) ABM method: Insulin $\mathbf{Y}(t)$ dynamics at $\mathbf{Y}_{\text{in}} = 0$ for fractional orders $\nu = 0.7, 0.75, 0.85, 0.95, 1$

(b) GRKM method: Insulin $\mathbf{Y}(t)$ dynamics at $\mathbf{Y}_{\text{in}} = 0$ for fractional orders $\nu = 0.7, 0.75, 0.85, 0.95, 1$

Figure 11. Comparison of $\mathbf{Y}(t)$ dynamics under ABM and GRKM at $\mathbf{Y}_{\text{in}} = 0$ for fractional orders $\nu = 0.7, 0.75, 0.85, 0.95, 1$. (a) ABM insulin reflects only endogenous secretion. (b) GRKM insulin shows comparable endogenous dynamics.

6.2. Comparison between SRKM and GRKM

In this study we use the SRK4 numerical method to solve the stochastic structural model (1.2), including the assumption of initial data, $(\mathbf{Y}_0, \mathbf{X}_0) = (128.052, 0)$. This method is used to compare the fractional stochastic and deterministic diabetes model for different noise intensities (0.1, 0.3, 0.6, 0.8, 1.0, 1.2) and insulin input rates ($\mathbf{Y}_{\text{in}} = 0, 3$). It can be seen in Figures 12–24 that the SRK4 numerical approximation method effectively compares the stochastic and deterministic dynamics.

Figures 12 through 24 examine the differences between the fractional stochastic and fractional deterministic diabetes models across varying noise levels. The stochastic model is solved using the SRK4 method to approximate glucose-insulin dynamics, incorporating real-world fluctuations. The deterministic model follows a smooth trajectory (red dashed line), representing an idealized case without random disturbances. In contrast, the stochastic model introduces Gaussian white noise, which captures biological variability more effectively. Shaded regions represent 95% confidence intervals computed over multiple stochastic realizations.

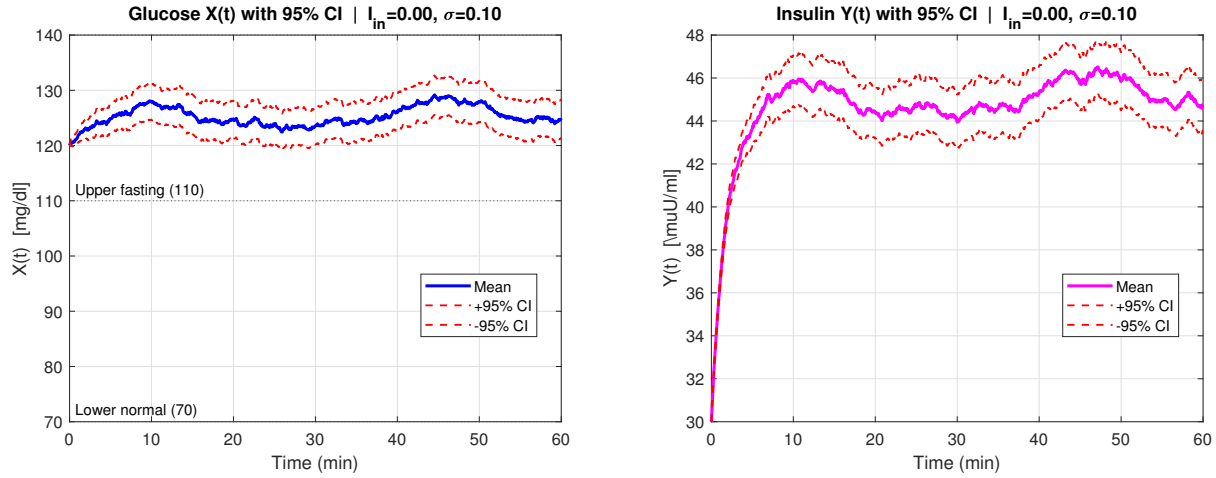

(a) Stochastic glucose $\mathbf{X}(t)$ with 95% CI at $\mathbf{Y}_{\text{in}} = 0$, $\sigma = 0.1$. Deterministic baseline (red dashed) shows idealized trajectory.

(b) Stochastic insulin $\mathbf{Y}(t)$ with 95% CI at $\mathbf{Y}_{\text{in}} = 0$, $\sigma = 0.1$. Deterministic insulin response (red dashed) with stochastic fluctuations.

Figure 12. Comparison of stochastic (SRK4) and deterministic (GRKM) dynamics at $\mathbf{Y}_{\text{in}} = 0$ with noise intensity $\sigma = 0.1$. (a) Glucose $\mathbf{X}(t)$ showing minimal stochastic variation around deterministic baseline. (b) Insulin $\mathbf{Y}(t)$ with narrow confidence intervals. Shaded regions indicate 95% confidence intervals computed over 1000 realizations.

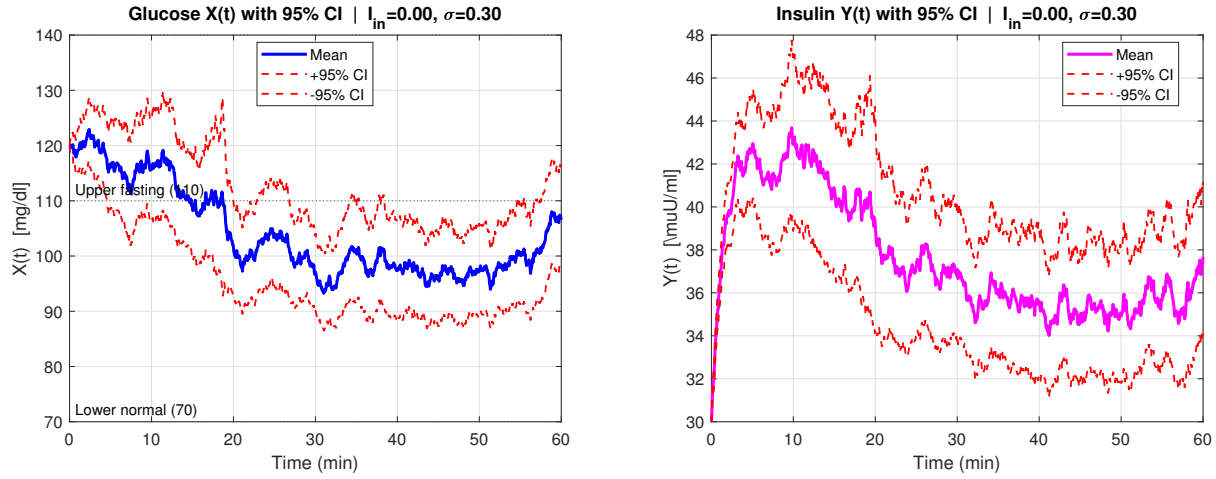

(a) Stochastic glucose $\mathbf{X}(t)$ with 95% CI at $\mathbf{Y}_{\text{in}} = 0$, $\sigma = 0.3$. Increased noise amplitude produces wider confidence bands.

(b) Stochastic insulin $\mathbf{Y}(t)$ with 95% CI at $\mathbf{Y}_{\text{in}} = 0$, $\sigma = 0.3$. Insulin variability increases proportionally with noise intensity.

Figure 13. Comparison of stochastic and deterministic dynamics at $\mathbf{Y}_{\text{in}} = 0$ with noise intensity $\sigma = 0.3$. (a) Glucose $\mathbf{X}(t)$ with moderate stochastic fluctuations. (b) Insulin $\mathbf{Y}(t)$ showing increased variability.

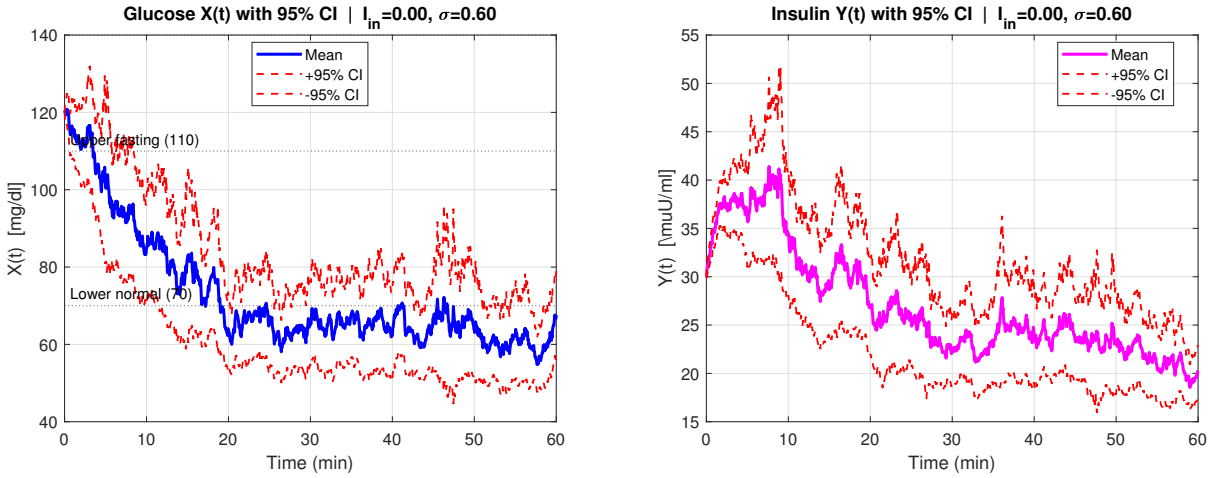

(a) Stochastic glucose $\mathbf{X}(t)$ with 95% CI at $\mathbf{Y}_{\text{in}} = 0$, $\sigma = 0.6$. Glucose fluctuations now span from normal to impaired fasting range. (b) Stochastic insulin $\mathbf{Y}(t)$ with 95% CI at $\mathbf{Y}_{\text{in}} = 0$, $\sigma = 0.6$. Insulin confidence intervals broaden substantially.

Figure 14. Comparison of stochastic and deterministic dynamics at $\mathbf{Y}_{\text{in}} = 0$ with noise intensity $\sigma = 0.6$. (a) Glucose $\mathbf{X}(t)$ exhibiting clinically significant variability. (b) Insulin $\mathbf{Y}(t)$ with corresponding fluctuations.

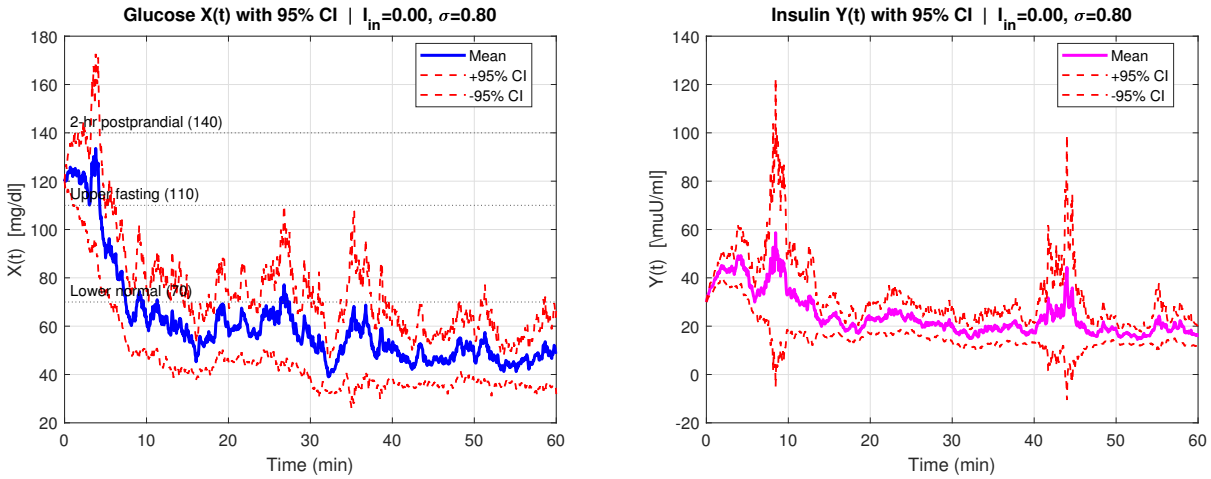

(a) Stochastic glucose $\mathbf{X}(t)$ with 95% CI at $\mathbf{Y}_{\text{in}} = 0$, $\sigma = 0.8$. Upper confidence bound approaches postprandial threshold (140 mg/dl). (b) Stochastic insulin $\mathbf{Y}(t)$ with 95% CI at $\mathbf{Y}_{\text{in}} = 0$, $\sigma = 0.8$. Insulin levels show wide dispersion including negative values truncated at zero.

Figure 15. Comparison of stochastic and deterministic dynamics at $\mathbf{Y}_{\text{in}} = 0$ with noise intensity $\sigma = 0.8$. (a) Glucose $\mathbf{X}(t)$ with substantial hyperglycemic excursions. (b) Insulin $\mathbf{Y}(t)$ with broad confidence region.

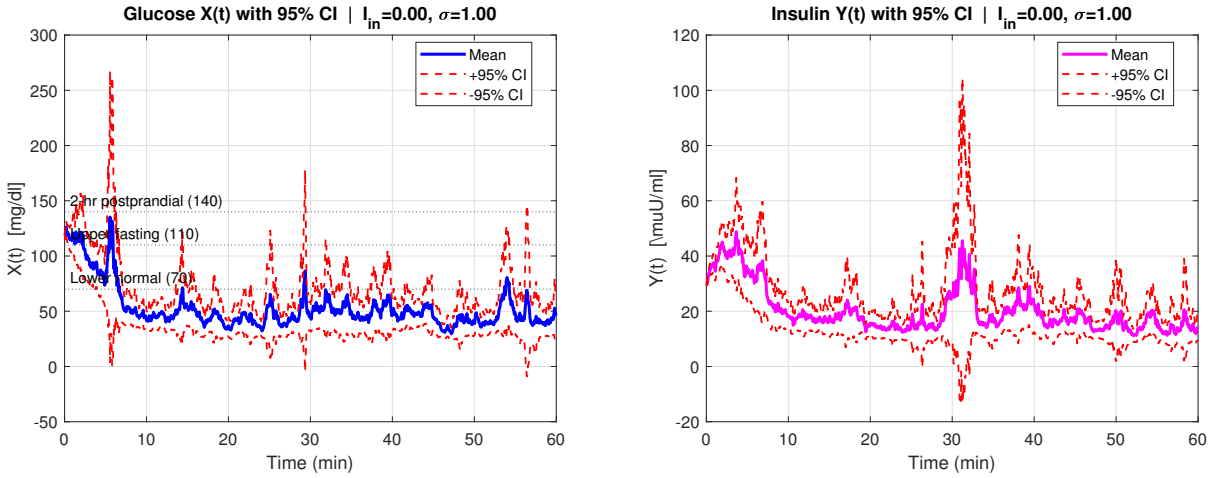

(a) Stochastic glucose $\mathbf{X}(t)$ with 95% CI at $\mathbf{Y}_{\text{in}} = 0$, $\sigma = 1.0$. Upper bound exceeds 140 mg/dl, indicating postprandial hyperglycemia risk.

(b) Stochastic insulin $\mathbf{Y}(t)$ with 95% CI at $\mathbf{Y}_{\text{in}} = 0$, $\sigma = 1.0$. Extreme variability in insulin dynamics.

Figure 16. Comparison of stochastic and deterministic dynamics at $\mathbf{Y}_{\text{in}} = 0$ with noise intensity $\sigma = 1.0$. (a) Glucose $\mathbf{X}(t)$ with high-amplitude fluctuations. (b) Insulin $\mathbf{Y}(t)$ with corresponding volatility.

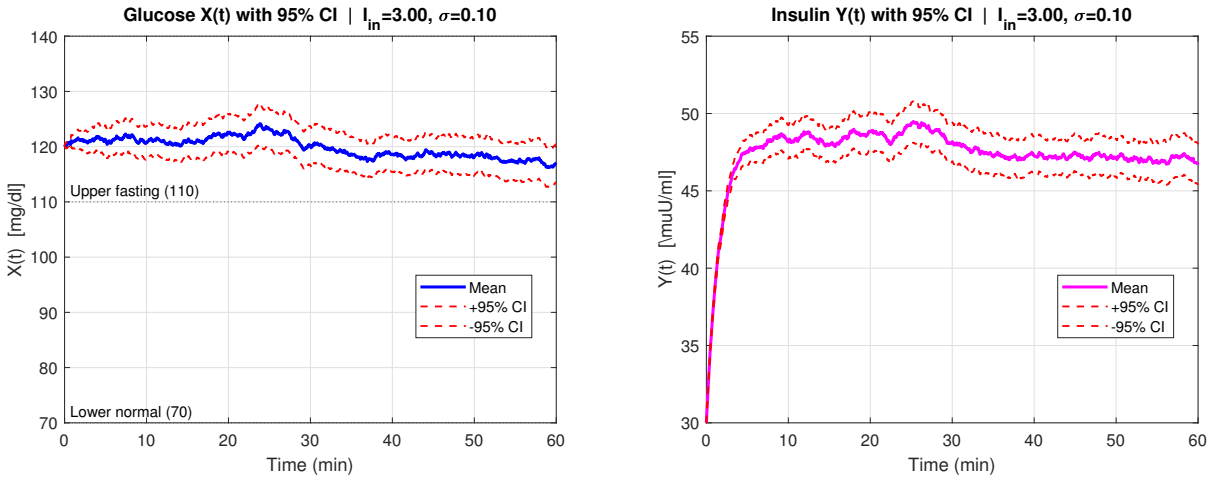

(a) Stochastic glucose $\mathbf{X}(t)$ with 95% CI at $\mathbf{Y}_{\text{in}} = 0$, $\sigma = 1.2$. Maximum noise condition produces extreme glycemic variability.

(b) Stochastic insulin $\mathbf{Y}(t)$ with 95% CI at $\mathbf{Y}_{\text{in}} = 0$, $\sigma = 1.2$. Insulin confidence interval spans from near-zero to supraphysiological levels.

Figure 17. Comparison of stochastic and deterministic dynamics at $\mathbf{Y}_{\text{in}} = 0$ with noise intensity $\sigma = 1.2$. (a) Glucose $\mathbf{X}(t)$ with maximum variability. (b) Insulin $\mathbf{Y}(t)$ showing unstable regulation.

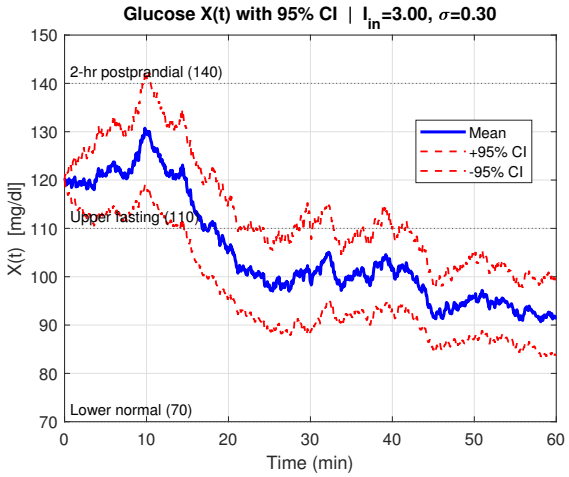

(a) Stochastic glucose $\mathbf{X}(t)$ with 95% CI at $\mathbf{Y}_{\text{in}} = 3$, $\sigma = 0.1$. Exogenous insulin reduces baseline glucose; minimal noise.

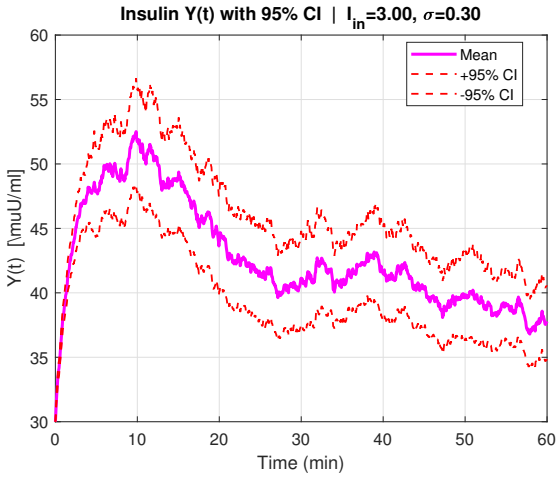

(b) Stochastic insulin $\mathbf{Y}(t)$ with 95% CI at $\mathbf{Y}_{\text{in}} = 3$, $\sigma = 0.1$. Elevated insulin baseline from exogenous administration.

Figure 18. Comparison of stochastic and deterministic dynamics at $\mathbf{Y}_{\text{in}} = 3$ with noise intensity $\sigma = 0.1$. (a) Glucose $\mathbf{X}(t)$ with exogenous insulin effect showing lower steady-state. (b) Insulin $\mathbf{Y}(t)$ with elevated baseline and minimal stochastic variation.

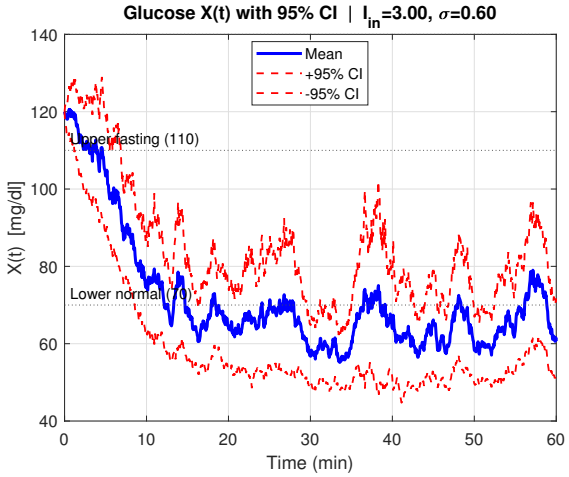

(a) Stochastic glucose $\mathbf{X}(t)$ with 95% CI at $\mathbf{Y}_{\text{in}} = 3$, $\sigma = 0.3$. Moderate fluctuations around reduced glucose baseline.

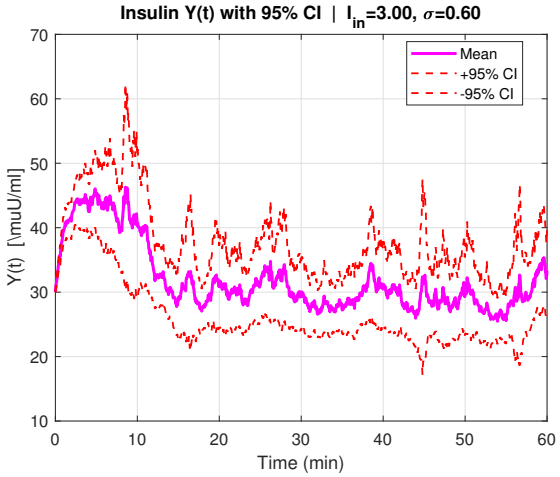

(b) Stochastic insulin $\mathbf{Y}(t)$ with 95% CI at $\mathbf{Y}_{\text{in}} = 3$, $\sigma = 0.3$. Insulin variability increases with noise intensity.

Figure 19. Comparison of stochastic and deterministic dynamics at $\mathbf{Y}_{\text{in}} = 3$ with noise intensity $\sigma = 0.3$. (a) Glucose $\mathbf{X}(t)$ with improved glycemic control. (b) Insulin $\mathbf{Y}(t)$ with moderate fluctuations.

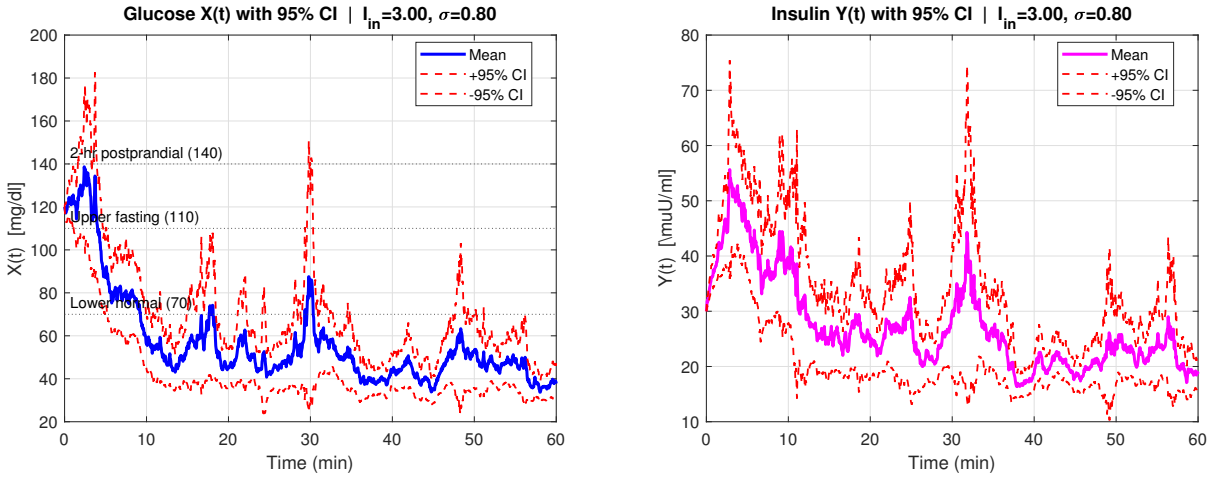

(a) Stochastic glucose $\mathbf{X}(t)$ with 95% CI at $\mathbf{Y}_{\text{in}} = 3$, $\sigma = 0.6$. Glucose remains within normal range despite increased noise.

(b) Stochastic insulin $\mathbf{Y}(t)$ with 95% CI at $\mathbf{Y}_{\text{in}} = 3$, $\sigma = 0.6$. Insulin confidence intervals widen at higher noise.

Figure 20. Comparison of stochastic and deterministic dynamics at $\mathbf{Y}_{\text{in}} = 3$ with noise intensity $\sigma = 0.6$. (a) Glucose $\mathbf{X}(t)$ maintaining normoglycemia. (b) Insulin $\mathbf{Y}(t)$ with amplified stochastic variation.

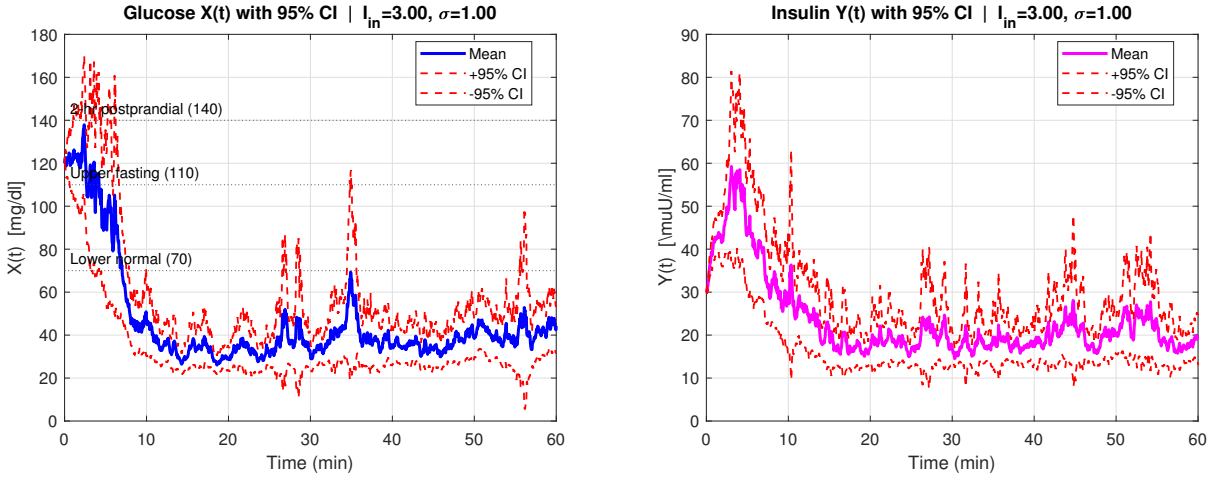

(a) Stochastic glucose $\mathbf{X}(t)$ with 95% CI at $\mathbf{Y}_{\text{in}} = 3$, $\sigma = 0.8$. Upper bound approaches fasting threshold with noise-induced excursions.

(b) Stochastic insulin $\mathbf{Y}(t)$ with 95% CI at $\mathbf{Y}_{\text{in}} = 3$, $\sigma = 0.8$. Pronounced insulin variability despite exogenous input.

Figure 21. Comparison of stochastic and deterministic dynamics at $\mathbf{Y}_{\text{in}} = 3$ with noise intensity $\sigma = 0.8$. (a) Glucose $\mathbf{X}(t)$ with borderline glycemic control. (b) Insulin $\mathbf{Y}(t)$ showing substantial stochastic fluctuations.

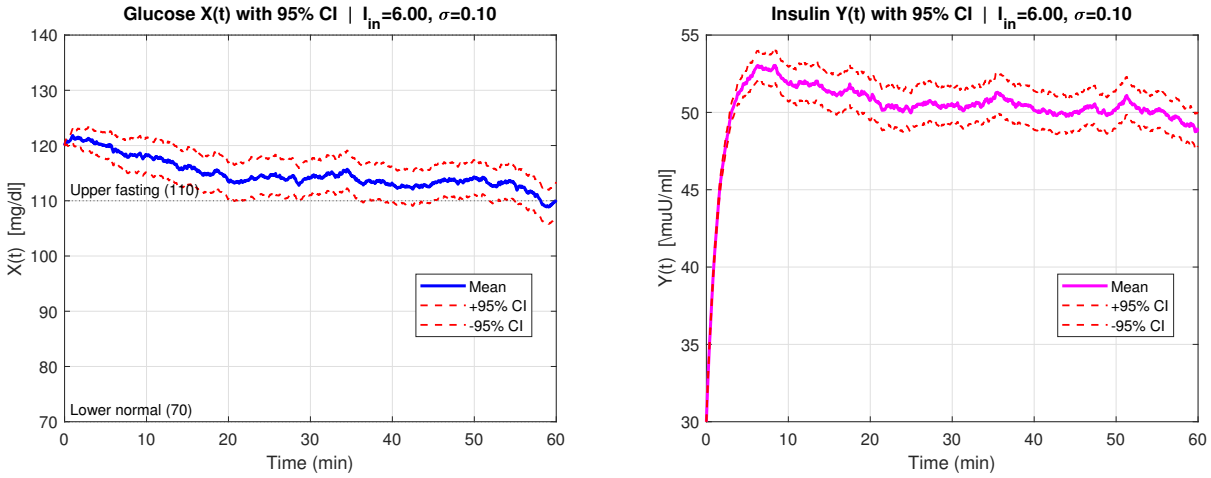

(a) Stochastic glucose $\mathbf{X}(t)$ with 95% CI at $\mathbf{Y}_{\text{in}} = 3$, $\sigma = 1.0$. Upper confidence bound exceeds normal fasting range.

(b) Stochastic insulin $\mathbf{Y}(t)$ with 95% CI at $\mathbf{Y}_{\text{in}} = 3$, $\sigma = 1.0$. High noise compromises insulin stability.

Figure 22. Comparison of stochastic and deterministic dynamics at $\mathbf{Y}_{\text{in}} = 3$ with noise intensity $\sigma = 1.0$. (a) Glucose $\mathbf{X}(t)$ with intermittent hyperglycemia. (b) Insulin $\mathbf{Y}(t)$ with large confidence intervals.

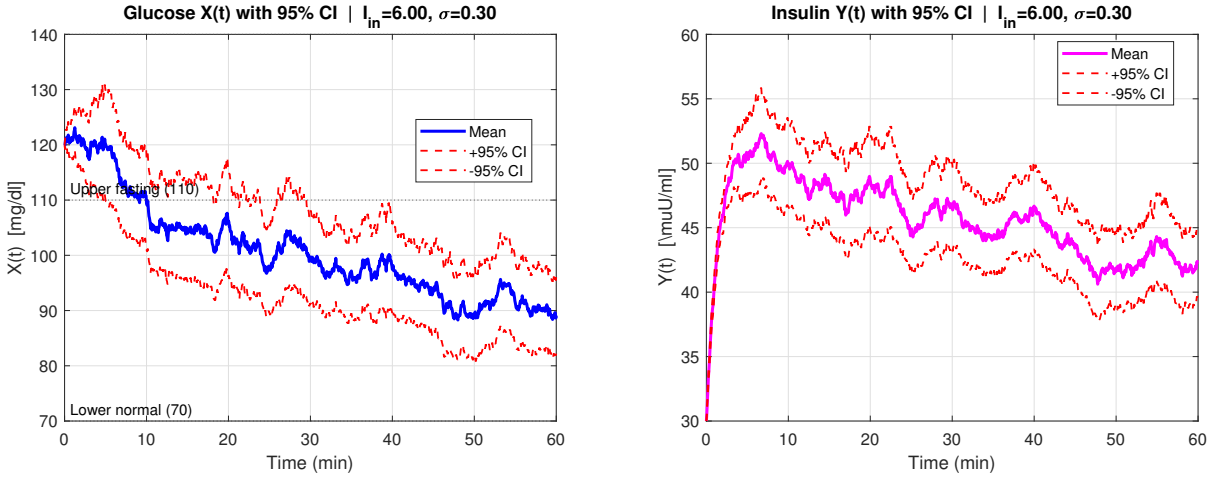

(a) Stochastic glucose $\mathbf{X}(t)$ with 95% CI at $\mathbf{Y}_{\text{in}} = 3$, $\sigma = 1.2$. Maximum noise produces clinically significant glucose variability.

(b) Stochastic insulin $\mathbf{Y}(t)$ with 95% CI at $\mathbf{Y}_{\text{in}} = 3$, $\sigma = 1.2$. Severe insulin fluctuations challenge metabolic stability.

Figure 23. Comparison of stochastic and deterministic dynamics at $\mathbf{Y}_{\text{in}} = 3$ with noise intensity $\sigma = 1.2$. (a) Glucose $\mathbf{X}(t)$ with extreme glycemic variability. (b) Insulin $\mathbf{Y}(t)$ demonstrating unstable feedback control.

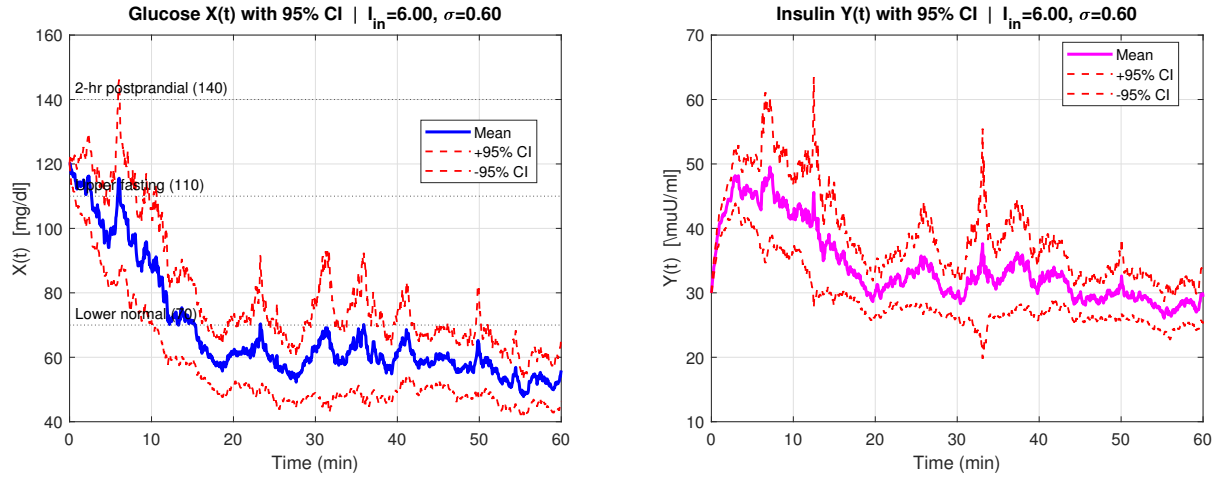

(a) Detailed stochastic glucose $\mathbf{X}(t)$ at $\mathbf{Y}_{\text{in}} = 3$, $\sigma = 0.8$. Enhanced visualization of confidence band structure.

(b) Detailed stochastic insulin $\mathbf{Y}(t)$ at $\mathbf{Y}_{\text{in}} = 3$, $\sigma = 0.8$. Magnified view of insulin variability patterns.

Figure 24. Detailed comparison of stochastic and deterministic dynamics at $\mathbf{Y}_{\text{in}} = 3$ with noise intensity $\sigma = 0.8$. (a) Glucose $\mathbf{X}(t)$ with enhanced resolution of stochastic band structure. (b) Insulin $\mathbf{Y}(t)$ showing detailed fluctuation patterns. This figure provides magnified visualization of the stochastic process.

As the noise level increases, fluctuations in glucose and insulin levels become more pronounced, aligning with real-life scenarios where glucose regulation is not perfectly maintained. Notably, higher noise intensities lead to greater glucose level deviations, demonstrating the role of biological randomness in diabetes management. Furthermore, the effect of insulin input ($\mathbf{Y}_{\text{in}}$) is evident, as increased insulin administration results in lower glucose levels, reinforcing insulin's regulatory function.

Overall, deterministic models provide a general trend of glucose-insulin interactions, while stochastic models offer a more realistic representation by accounting for random disturbances. As seen in stochastic models, increasing variability highlights the complexity of glucose-insulin regulation and the impact of uncertainty on real-world biological systems.

7. Discussion

Increased noise introduces significant variability in glucose and insulin dynamics. The stochastic model captures real-world fluctuations, accurately depicting physiological processes. Insulin injections lower glucose levels, and the reduction in glucose is proportional to the insulin injection rate. The deterministic model provides a smooth, idealized baseline, while the stochastic model reveals the impact of randomness and external factors on glucose and insulin dynamics.

The stochastic model enhances our understanding of patient-specific responses and glucose-insulin variability. Insights into insulin dosage effects can inform personalized treatment strategies, and the model can predict outcomes under different clinical scenarios, aiding diabetes management and treatment planning. Our results highlight the importance of incorporating stochastic elements in glucose-insulin modeling. The fractional deterministic model provides a clear baseline, whereas the

stochastic model demonstrates the significant impact of randomness and external perturbations. This combined approach advances our understanding and offers a comprehensive tool for diabetes management and research.

Deterministic glucose dynamics: The red dashed line represents deterministic glucose dynamics for each $\mathbf{Y}_{\text{in}}$ value. This line serves as a baseline, showing the idealized evolution of glucose levels over time. We observed that glucose levels decrease over time, reflecting the model's response to insulin and glucose intake.

Stochastic glucose dynamics: Colored lines represent the mean glucose levels at different noise intensities: 0.1, 0.3, 0.6, 0.8, 1.0, and 1.2. Increased noise results in significant glucose fluctuations, and the mean glucose level deviates more from the deterministic baseline as noise intensity increases. Higher noise levels introduce substantial variability, reflecting real-life physiological fluctuations. This variability directly impacts patient-specific glucose control and management. Without external insulin ($\mathbf{Y}_{\text{in}} = 0$), glucose remains elevated, indicating insufficient endogenous insulin. Increasing exogenous insulin to $\mathbf{Y}_{\text{in}} = 5$ and $\mathbf{Y}_{\text{in}} = 10$ produces a more pronounced reduction in glucose levels, and the extent of glucose reduction correlates positively with the insulin injection rate.

Deterministic insulin dynamics: The red dashed line represents the deterministic insulin dynamics for each $\mathbf{Y}_{\text{in}}$ value, showing the idealized evolution of insulin levels over time. Insulin levels adjust dynamically based on glucose concentrations and exogenous insulin administration.

8. Conclusions

This study introduces a fractional glucose-insulin model incorporating the Michaelis-Menten function to describe insulin degradation, providing a sophisticated approach to modeling diabetes pathology. The model's theoretical foundation is robust, establishing the existence, uniqueness, boundedness, nonnegativity, and stability of its solutions. Our analysis confirms the existence of an asymptotically stable global positive equilibrium, and Hyers-Ulam stability validates the model's robustness to small perturbations. Four strategic interventions based on parameter sensitivity analysis offer practical pathways for personalized diabetes management.

The fractional stochastic model of glucose-insulin degradation developed here has significant practical applications. It can simulate individual patient responses under various treatment regimens, aiding in the personalization of insulin therapy. Furthermore, the model can be integrated into model predictive control (MPC) algorithms for artificial pancreas systems, enhancing real-time glucose regulation in type 1 diabetes. The sensitivity analysis and control strategies presented in Section 4 provide clinicians with a quantitative framework to adjust treatment parameters based on patient-specific characteristics. By capturing both memory effects and inherent randomness, the model offers a more realistic representation of glucose-insulin dynamics than deterministic or integer-order models. Thus, this work not only advances theoretical understanding but also contributes to the development of more effective, personalized diabetes management tools.

Future work will extend the model to incorporate additional physiological complexities, such as time delays and hormonal counter-regulations, and explore its applicability to other metabolic disorders.

Author Contributions

Sayed Saber: Conceptualization, methodology, formal analysis, theoretical investigation (existence, uniqueness, stability, and Hyers-Ulam stability analysis), development of the fractional stochastic model, numerical implementation (ABM, GRKM, and SRK4 methods), supervision, manuscript drafting, and final revision; Emad Solouma: Mathematical modeling, validation of analytical results, assistance with stability analysis and Lyapunov framework, interpretation of biological implications, and critical revision of the manuscript; A. F. Aljohani: Numerical simulations, parameter calibration, sensitivity analysis, graphical visualization of results, and verification of computational accuracy; Faisal Muteb K. Almalki: Literature review, stability, data interpretation, clinical relevance assessment, proofreading, formatting, and manuscript editing.

All authors have read and approved the final version of the manuscript and agree to be accountable for all aspects of the work.

Use of Generative-AI tools declaration

The authors declare they have not used Artificial Intelligence (AI) tools in the creation of this article.

Funding

This work was supported and funded by the Deanship of Scientific Research at Imam Mohammad Ibn Saud Islamic University (IMSIU) (grant number IMSIU-DDRSP2601).

Conflict of interest

The authors declare that they have no conflict of interest.

References

1. J. Li, Y. Kuang, C. C. Mason, Modeling the glucose-insulin regulatory system and ultradian insulin secretory oscillations with two time delays, *J. Theor. Biol.*, **242** (2006), 722–735. https://doi.org/10.1016/j.jtbi.2006.04.002
2. B. Topp, K. Promislow, G. Devries, R. M. Miura, D. T. Finegood, A model of β-cell mass, insulin, and glucose, *J. Theor. Biol.*, **206** (2000), 605–619. https://doi.org/10.1006/jtbi.2000.2150
3. H. Wang, J. Li, Y. Kuang, Mathematical modeling and qualitative analysis of insulin therapies, *Math. Biosci.*, **210** (2007), 17–33. https://doi.org/10.1016/j.mbs.2007.05.008
4. H. Wang, J. Li, Y. Kuang, Enhanced modelling of the glucose-insulin system and its applications in insulin therapies, *J. Biol. Dyn.*, **3** (2009), 22–38. https://doi.org/10.1080/17513750802101927
5. M. Ma, J. Li, Dynamics of a glucose-insulin model, *J. Biol. Dyn.*, **16** (2022), 733–745. https://doi.org/10.1080/17513758.2022.2146769
6. S. Saber, E. B. M. Bashier, S. M. Alzahrani, I. A. Noaman, A mathematical model of glucose-insulin interaction with time delay, *J. Appl. Comput. Math.*, **7** (2018), 416–421. https://doi.org/10.4172/2168-9679.1000416

7. M. H. Alshehri, F. Z. Duraihem, A. Alalyani, S. Saber, A Caputo (discretization) fractional-order model of glucose-insulin interaction: Numerical solution and comparisons with experimental data, *J. Taibah Univ. Sci.*, **15** (2021), 26–36. https://doi.org/10.1080/16583655.2021.1872197
8. K. I. A. Ahmed, S. M. Mirgani, A. Seadawy, S. Saber, A comprehensive investigation of fractional glucose-insulin dynamics: Existence, stability, and numerical comparisons using residual power series and generalized Runge-Kutta methods, *J. Taibah Univ. Sci.*, **19** (2025), 2460280. https://doi.org/10.1080/16583655.2025.2460280
9. M. H. Alshehri, S. Saber, F. Z. Duraihem, Dynamical analysis of fractional-order of IVGTT glucose-insulin interaction, *Int. J. Nonlin. Sci. Num.*, **24** (2023), 1123–1140. https://doi.org/10.1515/ijnsns-2020-0201
10. S. Saber, A. Alalyani, Stability analysis and numerical simulations of IVGTT glucose-insulin interaction models with two time delays, *Math. Model. Anal.*, **27** (2022), 383–407. https://doi.org/10.3846/mma.2022.14007
11. K. I. A. Ahmed, H. D. S. Adam, M. Y. Youssif, S. Saber, Different strategies for diabetes by mathematical modeling: Modified minimal model, *Alex. Eng. J.*, **80** (2023), 74–87. https://doi.org/10.1016/j.aej.2023.07.050
12. K. I. A. Ahmed, D. S. A. Adam, M. Y. Youssif, S. Saber, Different strategies for diabetes by mathematical modeling: Applications of fractal-fractional derivatives in the sense of Atangana-Baleanu, *Results Phys.*, **52** (2023), 106892. https://doi.org/10.1016/j.rinp.2023.106892
13. R. Caponetto, G. Dongola, L. Fortuna, I. Petras, *Fractional order systems: Modelling and control applications*, World Scientific, 2010. https://doi.org/10.1142/7709
14. S. B. Minucci, R. L. Heise, A. M. Reynolds, Review of mathematical modeling of the inflammatory response in lung infections and injuries, *Front. Appl. Math. Stat.* **6** (2020), 1–25. https://doi.org/10.3389/fams.2020.00036
15. M. A. Dokuyucu, E. Çelik, H. Bulut, H. M. Baskonus, Cancer treatment model with the Caputo-Fabrizio fractional derivative, *Eur. Phys. J. Plus*, **133** (2018), 92. https://doi.org/10.1140/epjp/i2018-11950-y
16. M. F. Faraloya, S. Shafie, F. M. Siam, R. Mahmud, S. O. Ajadi, Numerical simulation and optimization of radiotherapy cancer treatments using the Caputo fractional derivative, *Malays. J. Math. Sci.* **15** (2021), 161–187.
17. A. Alalyani, S. Saber, Stability analysis and numerical simulations of the fractional COVID-19 pandemic model, *Int. J. Nonlin. Sci. Num.* **24** (2023), 989–1002. https://doi.org/10.1515/ijnsns-2021-0042
18. S. Saber, A. M. Alghamdi, G. A. Ahmed, K. M. Alshehri, Mathematical modelling and optimal control of pneumonia disease in sheep and goats in Al-Baha region with cost-effective strategies, *AIMS Math.*, **7** (2022), 12011–12049. https://doi.org/10.3934/math.2022669
19. S. M. Al-Zahrani, F. E. I. Elsmih, K. S. Al-Zahrani, S. Saber, A fractional order SITR model for forecasting of transmission of COVID-19: Sensitivity statistical analysis, *Malays. J. Math. Sci.*, **16** (2022), 517–536. https://doi.org/10.47836/mjms.16.3.08
20. S. Saber, Solution to $\bar{\partial}$-problem with support conditions in weakly q-convex domains, *Commun. Korean Math. Soc.*, **33** (2018), 409–421. https://doi.org/10.4134/CKMS.c170022

21. S. Saber, Solvability of the tangential Cauchy-Riemann equations on boundaries of strictly q-convex domains, *Lobachevskii J. Math.*, **32** (2011), 189–193. https://doi.org/10.1134/S1995080211030115
22. M. Althubyani, H. D. S. Adam, A. Alalyani, N. E. Taha, K. O. Taha, R. A. Alharbi, S. Saber, Understanding zoonotic disease spread with a fractional order epidemic model, *Sci. Rep.*, **15** (2025), 13921. https://doi.org/10.1038/s41598-025-95943-6
23. H. D. S. Adam, M. Althubyani, S. M. Mirgani, S. Saber, An application of Newton's interpolation polynomials to the zoonotic disease transmission between humans and baboons system based on a time-fractal fractional derivative with a power-law kernel, *AIP Adv.*, **15** (2025), 045217. https://doi.org/10.1063/5.0253869
24. M. Alhazmi, S. Saber, Glucose-insulin regulatory system: Chaos control and stability analysis via Atangana-Baleanu fractal-fractional derivatives, *Alex. Eng. J.*, **122** (2025), 77–90. https://doi.org/10.1016/j.aej.2025.02.066
25. S. Saber, L^2 estimates and existence theorems for $\bar{\partial}_b$ on Lipschitz boundaries of Q-pseudoconvex domains, *C. R. Math.*, **358** (2020), 435–458. https://doi.org/10.5802/crmath.43
26. N. Almutairi, S. Saber, Application of a time-fractal fractional derivative with a power-law kernel to the Burke-Shaw system based on Newton's interpolation polynomials, *MethodsX*, **12** (2024), 102510. https://doi.org/10.1016/j.mex.2023.102510
27. S. Saber, Control of chaos in the Burke-Shaw system of fractal-fractional order in the sense of Caputo-Fabrizio, *J. Appl. Math. Comput. Mech.*, **23** (2024), 83–96. https://doi.org/10.17512/jamcm.2024.1.07
28. N. Almutairi, S. Saber, Existence of chaos and the approximate solution of the Lorenz-Lü-Chen system with the Caputo fractional operator, *AIP Adv.*, **14** (2024), 015112. https://doi.org/10.1063/5.0185906
29. K. I. A. Ahmed, H. D. S. Adam, N. Almutairi, S. Saber, Analytical solutions for a class of variable-order fractional Liu system under time-dependent variable coefficients, *Results Phys.*, **56** (2024), 107311. https://doi.org/10.1016/j.rinp.2023.107311
30. N. Almutairi, S. Saber, On chaos control of nonlinear fractional Newton-Leipnik system via fractional Caputo-Fabrizio derivatives, *Sci. Rep.*, **13** (2023), 22726. https://doi.org/10.1038/s41598-023-49541-z
31. N. Almutairi, S. Saber, H. Ahmad, The fractal-fractional Atangana-Baleanu operator for pneumonia disease: Stability, statistical and numerical analyses, *AIMS Math.*, **8** (2023), 29382–29410. https://doi.org/10.3934/math.20231504
32. N. Almutairi, S. Saber, Chaos control and numerical solution of time-varying fractional Newton-Leipnik system using fractional Atangana–Baleanu derivatives, *AIMS Math.*, **8** (2023), 25863–25887. https://doi.org/10.3934/math.20231319
33. S. K. Choi, B. Kang, N. Koo, Stability for Caputo fractional differential systems, *Abstr. Appl. Anal.*, **2014** (2014), 631419. https://doi.org/10.1155/2014/631419
34. A. Boukhouima, K. Hattaf, N. Yousfi, Dynamics of a fractional order HIV infection model with specific functional response and cure rate, *Int. J. Differ. Equ.*, **2017** (2017), 8372140. https://doi.org/10.1155/2017/8372140

35. J. P. La Salle, *The stability of dynamical systems*, Society for Industrial and Applied Mathematics, 1976.

36. H. L. Li, L. Zhang, C. Hu, Y. Jiang, Z. Teng, Dynamical analysis of a fractional-order predator-prey model incorporating a prey refuge, *J. Appl. Math. Comput.*, **54** (2017), 435–449. https://doi.org/10.1007/s12190-016-1017-8

37. I. Podlubny, *Fractional differential equations*, 1999.

38. X. Mao, *Stochastic differential equations and applications*, 1997.

39. H. D. S. Adam, K. I. Adam, S. Saber, G. Farid, Existence theorems for the $\bar{\partial}$ equation and Sobolev estimates on q-convex domains, *AIMS Math.*, **8** (2023), 31141–31157. https://doi.org/10.3934/math.20231594

40. X. Zhong, S. Guo, M. Peng, Stability of stochastic SIRS epidemic models with saturated incidence rates and delay, *Stoch. Anal. Appl.*, **35** (2017), 1–26. https://doi.org/10.1080/07362994.2016.1244644

41. T. Khan, I. H. Jung, G. Zaman, A stochastic model for the transmission dynamics of hepatitis B virus, *J. Biol. Dyn.*, **13** (2019), 328–344. https://doi.org/10.1080/17513758.2019.1600750

42. A. Din, A. Khan, D. Baleanu, Stationary distribution and extinction of stochastic coronavirus (COVID-19) epidemic model, *Chaos Soliton. Fract.*, **139** (2020), 110036. https://doi.org/10.1016/j.chaos.2020.110036

43. M. Otero, H. G. Solari, Stochastic eco-epidemiological model of dengue disease transmission by *Aedes aegypti* mosquito, *Math. Biosci.*, **223** (2010), 32–46. https://doi.org/10.1016/j.mbs.2009.10.005

44. H. Woodall, B. Adams, Stochastic modelling for age-structured dengue epidemiology with and without seasonal variation, In: *9th European Conference on Mathematical and Theoretical Biology*, 2014.

45. T. Khan, A. Khan, G. Zaman, The extinction and persistence of the stochastic hepatitis B epidemic model, *Chaos Soliton. Fract.*, **108** (2018), 123–128. https://doi.org/10.1016/j.chaos.2018.01.036

46. A. Atangana, B. Dumitru, New fractional derivatives with nonlocal and non-singular kernel: Theory and application to heat transfer model, *Therm. Sci.*, **20** (2016), 763–769. https://doi.org/10.2298/TSCI160111018A

47. M. Sivashankar, S. Sabarinathan, K. S. Nisar, C. Ravichandran, B. V. Senthil Kumar, Some properties and stability of Helmholtz model involved with nonlinear fractional difference equations and its relevance with quadcopter, *Chaos Soliton. Fract.*, **168** (2023), 113161. https://doi.org/10.1016/j.chaos.2023.113161

48. N. I. Okposo, E. Addai, J. S. Apanapudor, J. F. Gómez-Aguilar, A study on a monkeypox transmission model within the scope of fractal-fractional derivative with power-law kernel, *Eur. Phys. J. Plus*, **138** (2023), 684. https://doi.org/10.1140/epjp/s13360-023-04334-1

49. J. Alzabut, R. Dhineshbabu, A. G. M. Selvam, J. F. Gómez-Aguilar, H. Khan, Existence, uniqueness and synchronization of a fractional tumor growth model in discrete time with numerical results, *Results Phys.*, **54** (2023), 107030. https://doi.org/10.1016/j.rinp.2023.107030

50. X. J. Yang, *Local fractional functional analysis and its applications*, Hong Kong: Asian Academic Publisher, 2011.

51. M. Mohammad, M. Saadaoui, A new fractional derivative extending classical concepts: Theory and applications, *Part. Differ. Equ. Appl. Math.*, **11** (2024), 100889. https://doi.org/10.1016/j.padiff.2024.100889
52. K. M. Saad, New fractional derivative with non-singular kernel for deriving Legendre spectral collocation method, *Alex. Eng. J.*, **59** (2020), 1909–1917. https://doi.org/10.1016/j.aej.2019.11.017
53. J. V. da C. Sousa, E. Capelas de Oliveira, A new truncated M-fractional derivative type unifying some fractional derivative types with classical properties, *Int. J. Anal. Appl.*, **16** (2018), 83–96. https://doi.org/10.28924/2291-8639-16-2018-83
54. R. Khalil, M. Al Horani, A. Yousef, M. Sababheh, A new definition of fractional derivative, *J. Comput. Appl. Math.*, **264** (2014), 65–70. https://doi.org/10.1016/j.cam.2014.01.002
55. R. Almeida, A. B. Malinowska, M. T. T. Monteiro, Fractional differential equations with a Caputo derivative with respect to a kernel function and their applications, *Math. Method. Appl. Sci.*, **41** (2018), 336–352. https://doi.org/10.1002/mma.4617
56. Y. H. Liang, K. J. Wang, Dynamics of new exact wave solutions to the local fractional Vakhnenko-Parkes equation, *Fractals*, **34** (2026), 2550102. https://doi.org/10.1142/S0218348X25501026
57. K. J. Wang, The fractal active low-pass filter within the local fractional derivative on the Cantor set, *COMPEL*, **42** (2023), 1396–1407. https://doi.org/10.1108/COMPEL-09-2022-0326
58. W. Liu, Q. Zuo, C. Xu, Finite-time and global Mittag-Leffler stability of fractional-order neural networks with S-type distributed delays, *AIMS Math.*, **9** (2024), 8339–8352. https://doi.org/10.3934/math.2024405
59. D. Xu, W. Liu, Stochastic asymptotic stability for stochastic inertial Cohen-Grossberg neural networks with time-varying delay, *J. Comput. Methods Sci.*, **23** (2023), 921–931. https://doi.org/10.3233/JCM-226480
60. Y. Zhang, Z. Li, W. Jiang, W. Liu, Exponential stability of stochastic inertial Cohen-Grossberg neural networks, *Int. J. Pattern Recogn.*, **37** (2023), 2259032. https://doi.org/10.1142/S0218001422590327
61. S. M. Ulam, *A collection of mathematical problems*, 1960.
62. S. M. Ulam, *Problems in modern mathematics*, Courier Corporation, 2004.
63. K. Diethelm, N. J. Ford, A. D. Freed, A predictor-corrector approach for the numerical solution of fractional differential equations, *Nonlinear Dyn.*, **29** (2002), 3–22. https://doi.org/10.1023/A:1016592219341
64. P. E. Kloeden, E. Platen, *Numerical solution of stochastic differential equations*, Berlin: Springer, 1999. https://doi.org/10.1007/978-3-662-12616-5